Strong influence of Black Carbon on aerosol optical properties in Central Amazonia during the fire season

Rafael Stern[1], Joel F. de Brito[2], Samara Carbone[3], Luciana Varanda Rizzo[4], Jonathan Daniel Muller[5] and Paulo Artaxo[4]

[1]Climate and Environment Department, National Institute of ~~Amazon~~Amazonia Research, Manaus, 69060-001, Brazil
[2]IMT Nord Europe, Institut Mines-Télécom, Université de Lille, Centre for Energy and Environment, 59000, Lille, France
[3]Agrarian Sciences Institute, Federal University of Uberlandia, Uberlandia, Brazil
[4]Physics Institute, University of São Paulo, 05508-090, Brazil
[5]School for Climate Studies, Stellenbosch University, Stellenbosch, South Africa

Correspondence to: Rafael Stern (rafa.stern@yahoo.com.br)

Abstract. During the dry season, the Amazonian atmosphere is strongly impacted by fires, even in remote areas. However, there are still knowledge gaps regarding how each aerosol type affects the aerosol radiative forcing. This work characterizes the chemical composition of submicrometer aerosols and source apportionment of Organic Aerosols (OA) and Equivalent Black Carbon (eBC) to study their influence on light scattering and absorption at a remote site in central Amazonia during the dry season (August-December 2013). We applied Positive Matrix Factorization (PMF) and multi-linear regression models to estimate chemical-dependent mass scattering (MSE) and extinction (MEE) efficiencies. Mean PM1 aerosol mass loading was 6.3±3.3 μg m^{-3}, with 77% of organics, grouped into 3 factors: Biomass Burning OA (BBOA), Isoprene derived Epoxydiol-Secondary OA (IEPOX-SOA) and Oxygenated OA (OOA). The bulk scattering and absorption coefficients at 637 nm were 17±10 Mm^{-1} and 3±2 Mm^{-1}, yielding a single scattering albedo of 0.87±0.03. Although eBC represented only 6% of the PM1 mass loading, MSE was highest for the eBC (13.58-7.62 m^2 g^{-1} at 450-700 nm), followed by BBOA (7.96-3.10 m^2 g^{-1}) and ammonium sulfate (AS, 4.79-4.58 m^2 g^{-1}). MEE was dominated by eBC (30.8%), followed by the OOA (19.9%) and AS (17.6%). The dominance of eBC over light scattering, in addition to absorption, depicts a ~~surprisingly~~remarkably high role of this important climate agent, ~~indicating the need~~with potentially broad implications for more precise radiative forcing quantification, increasing climate modelling precision, representing deep contributions to ~~further investigate the chemical processing and interaction between natural and anthropogenic aerosol sources over remote tropical forested areas.~~ Earth's climate system comprehension.

Style Definition: Normal: (Complex) Hebrew
Style Definition: Heading 2: (Complex) Hebrew
Style Definition: Heading 3: (Complex) Hebrew
Style Definition: Heading 4: (Complex) Hebrew
Style Definition: Bullets: (Complex) Hebrew, Indent: Bef 0", First line: 0", Outline numbered + Level: 1 + Numberi Style: 1, 2, 3, … + Start at: 1 + Alignment: Left + Aligned 0" + Tab after: 0.5" + Indent at: 0.5", Tab stops: 0.25", tab
Style Definition: Revision: (Complex) Hebrew, Justified, spacing: 1.5 lines
Formatted: Font: 17 pt, Bold, Font color: Black
Formatted
Formatted: Font: 12 pt, Font color: Black
Formatted: Font color: Black
Formatted: Font color: Black
Formatted: Font color: Black, English (United Kingdom)
Formatted: Font color: Black
Formatted: Font color: Black, English (United Kingdom)
Formatted: Font color: Black
Formatted: Font color: Black, English (United Kingdom)
Formatted: Font color: Black
Formatted: English (United Kingdom)
Formatted: English (United Kingdom)
Formatted
Formatted: English (United Kingdom)
Formatted: English (United Kingdom)
Formatted
Formatted: English (United Kingdom)
Formatted
Formatted: English (United Kingdom)
Formatted
Formatted: English (United Kingdom)
Formatted
Formatted: English (United Kingdom)
Formatted: English (United Kingdom)
Formatted: English (United Kingdom)
Formatted: English (United Kingdom)
Formatted: Font color: Black
Formatted

1 Introduction

The Amazon is the largest hydrologic basin and contiguous tropical forest area of the planet, representing important carbon reserves, sources of freshwater, and housing a large biodiversity (Andreae et al., 2015; Artaxo et al., 2013; Davidson et al., 2012; Pöhlker et al., 2016). The strong coupling between climate and the biological functioning of the forest is a key factor in the maintenance of the Amazonian ecosystem (Martin et al., 2010b; Pohlker et al., 2012). The Amazonian atmosphere is considered an important reactor, regulating its physical properties and chemical composition due to the high insolation and humidity (Andreae, 2001). Despite the high temperatures, precipitation rates, and insolation during most of the year, an annual cycle can be observed, with a wetter and less warm season and a drier and hotter season, whose length and period vary depending on the region of the Amazon (Marengo et al., 2001).

During the wet season, the Amazonian atmosphere represents one of the few continental regions with episodic atmospheric composition near pristine conditions (Andreae et al., 2015; Martin et al., 2010b; Pöhlker et al., 2018; Pöschl et al., 2010). Particle number concentration during the cleanest period is a few hundred particles cm^{-3}, very similar to remote oceanic regions (Andreae et al., 2015; Artaxo et al., 2013; Martin et al., 2010). However, during the dry season, forest fires are provoked in order to clear forest areas for agriculture, and also as part of pasture and cropland management (Aragão et al., 2016; Berenguer et al., 2021; Davidson et al., 2012). During these periods, forest fire emissions coupled with smaller rates of aerosol scavenging lead to particle number concentration increases by a factor of 10 in remote forest areas (Artaxo et al., 2013; Pöhlker et al., 2018). These stark seasonal differences in aerosol loading and composition have the potential to significantly modify the coupling biosphere-atmosphere (Zaveri et al., 2022), which is expected to be exacerbated in the future due to extreme climatic events in Amazonia (Flores et al., 2024).

Atmospheric aerosol particles influence climate through scattering and absorption of solar radiation (aerosol-radiation interactions, ARI) and by affecting cloud formation and lifetime (aerosol-cloud interactions, ACI) (Forster et al., 2021). However, the magnitude and the signal of global radiative forcing of aerosols still represent one of the largest uncertainties in global climate models (Kuhn et al., 2010; Rizzo et al., 2013; Szopa et al., 2023). Uncertainties on the radiative forcing of individual aerosol components are even higher (Myhre et al., 2013), with a direct impact on the accuracy of future climatic scenarios (Forster et al., 2021). Carbonaceous aerosols (i.e. organic and black carbon) dominate the Amazonian atmosphere (Artaxo et al., 2013). While Organic Aerosol (OA) originates from both primary emissions, as well as secondary formation from gaseous precursors (Martin et al., 2010), black carbon is mostly primarily emitted from incomplete combustion, and in remote areas of the Amazon it is associated with Amazonian or transatlantic forest fires (Artaxo et al., 2013; Holanda et al., 2020). The sign and magnitude of the ARI forcing are dependent on several parameters such as particle origin, size distribution, mixture and age, notably affecting the light-absorbing component of OA, termed brown carbon (Laskin et al., 2015; Saturno et al., 2018b).

The secondary component of OA (SOA) in the Amazon has been shown to be a major component, notably during the wet season (Chen et al., 2015; Shrivastava et al., 2019). Isoprene (2-methyl-1,3-butadiene, C_5H_8) is the most abundant VOC emitted

Formatted: Font color: Black

Formatted: Normal, Border: Top: (No border), Bottom: (N border), Left: (No border), Right: (No border), Between : (border), Tab stops: 3.13", Centered + 6.27", Right

~~globally, mostly located in tropical forests such as the Amazon (Marais et al., 2016; Yáñez-Serrano et al., 2015). The formation of isoprene-derived Secondary Organic Aerosol (SOA) is a sequence of complex reactions and depends on different factors, such low concentrations of NO (a typical byproduct of fossil fuel combustion), and pre-existing aerosol particles where isoprene can condense on (Brito et al., 2018; Caravan et al., 2024; Marais et al., 2016; Nah et al., 2019). One of the dominating isoprene SOA pathways in the Amazon is through the OH attack, leading to hydroperoxy radicals and subsequently via the HO_2 pathway (Shrivastava et al., 2019; Wennberg et al., 2018). This pathway can lead to different low-volatility products generally termed IEPOX-SOA (Isoprene EPOXydiols-Secondary Organic Aerosol) (Allan et al., 2014; Hu et al., 2015; Surratt et al., 2010). Isoprene oxidation product mixing ratios were previously shown to be higher during the dry season above the forest canopy, likely due to the higher insolation and temperature during this period, which favors the oxidative capacity of the atmosphere and leaf emission potential (Yáñez-Serrano et al., 2015). IEPOX-SOA mass concentrations have been shown to be significantly reduced during polluted conditions, associated with suppression due to urban NO emissions (de Sá et al., 2017). Alternatively, a study in polluted urban plumes in West Africa found that SO_4 increase plays a larger role in enhancing IEPOX-SOA loadings than NO in suppressing it (Brito et al., 2018). Secondary oxidized aerosol particles have been demonstrated to be more efficient at scattering radiation than primary particles (Kleinman et al., 2020; Paredes-Miranda et al., 2009; Reid et al., 2005; Smith et al., 2020).~~

~~Chemical composition, processes, and sources of atmospheric aerosol particles in the Amazon have been widely studied during both the wet and dry seasons, in sites representing pristine conditions (Andreae et al., 2015; Chen et al., 2015; Martin et al., 2010a) as well as strongly impacted by fires and urban pollution (Brito et al., 2014; Ponczek et al., 2021; de Sá et al., 2018; Zaveri et al., 2022). Physical properties of radiation absorption and scattering were described (Artaxo et al., 2013; Nascimento et al., 2021; Palácios et al., 2020; Rizzo et al., 2013; de Sá et al., 2019; Sena et al., 2013). However, the intrinsic optical properties of each aerosol species are still rare (Velazquez-Garcia et al., 2023), notably associated with OA origins (Ponczek et al., 2021). Our study details the chemical properties of submicrometer aerosol particles in a forest site in central Amazonia during the dry season and their influence on radiation scattering and absorption. We applied positive matrix factorization (PMF) to the organic fraction, associated mass extinction, absorption, and scattering efficiencies to different aerosol components via multi-linear regression to improve our comprehension of their intrinsic properties, as well as estimate their role on aerosol-radiation interaction in Central Amazonia during the dry season.~~

The strong coupling between climate and the biological functioning of Amazonia is a key factor in the maintenance of its ecosystem (Martin et al., 2010b; Pöhlker et al., 2012). The Amazonian atmosphere is considered an important reactor, regulating its physical properties and chemical composition due to the high insolation and humidity (Andreae, 2001). However, during the dry season, forest fire emissions coupled with smaller rates of aerosol scavenging lead to particle number concentration increases by a factor of 10 in remote forest areas compared to near pristine conditions episodes during the wet season (Andreae et al., 2015; Artaxo et al., 2013; Pöhlker et al., 2018). These stark seasonal differences in aerosol loading and composition have the potential to significantly modify the biosphere-atmosphere coupling (Zaveri et al., 2022). These seasonal differences are expected to be exacerbated in the future due to extreme climatic events in Amazonia (Flores et al., 2024).

Formatted: Font color: Black

Formatted: Normal, Border: Top: (No border), Bottom: (N border), Left: (No border), Right: (No border), Between : (border), Tab stops: 3.13", Centered + 6.27", Right

Carbonaceous aerosols (i.e. organic aerosols, OA and black carbon, BC) dominate the atmosphere particles chemical classes in Amazonia (Artaxo et al., 2013). The secondary component of OA (SOA) has been shown to have a major contribution, notably during the wet season (Chen et al., 2015; Shrivastava et al., 2019). In remote regions of Amazonia, aged and highly processed oxygenated particles originated from multiple sources (forest fires, derived from volatile organic compounds – VOCs…) are a major component of basin-wide haze observed during biomass burning season (Darbyshire et al., 2019). Isoprene (2-methyl-1,3-butadiene, C_5H_8) is the most abundant VOC emitted globally, mostly in tropical forests (Marais et al., 2016; Yáñez-Serrano et al., 2015). The formation of isoprene-derived Secondary Organic Aerosol (SOA) is a sequence of complex reactions and depends on different factors, such low concentrations of NO and pre-existing aerosol particles where isoprene can condense on (Brito et al., 2018; Caravan et al., 2024; Marais et al., 2016; Nah et al., 2019). One of the dominating isoprene SOA pathways in Amazonia is through the OH attack, leading to hydroperoxy radicals (Shrivastava et al., 2019; Wennberg et al., 2018). This pathway can lead to different low-volatility products generally termed IEPOX-SOA (Isoprene EPOXydiols-Secondary Organic Aerosol) (Allan et al., 2014; Hu et al., 2015; Surratt et al., 2010). While OA originates from both primary emissions, as well as secondary formation from gaseous precursors (Martin et al., 2010b), BC is mostly primarily emitted from incomplete combustion, and in remote areas of Amazonia it is associated with regional or transatlantic forest fires (Artaxo et al., 2013; Holanda et al., 2020; Saturno et al., 2018a).

Atmospheric aerosol particles influence climate through scattering and absorption of solar radiation (aerosol-radiation interactions, ARI) and by affecting cloud formation and lifetime (aerosol-cloud interactions, ACI) (Forster et al., 2021). However, the magnitude and the signal of global radiative forcing of aerosols still represent one of the largest uncertainties in global climate models (Szopa et al., 2023). Uncertainties on the radiative forcing of individual aerosol components are even higher, with a direct impact on the accuracy of future climate scenarios (Forster et al., 2021). The sign and magnitude of the ARI forcing are dependent on several parameters such as particles size distribution, mixture, aging processes and meteorological conditions, as well as the particle chemical composition and its effect on the complex refractive index, based, among other factors, on the origin of the particles (Laskin et al., 2015; Li et al., 2024; Saturno et al., 2018a). Aerosol particles known for efficiently absorbing radiation - such as BC - often also exhibit significant scattering efficiencies, which are strongly influenced by their size, chemical composition, and the extent and nature of their atmospheric aging and coatings (Bond and Bergstrom, 2006; Schwarz et al., 2006; Yu et al., 2010). Although chemical aging has shown to enhance light absorption due to the coating of the BC core by condensing semi- and intermediate volatility organic compounds or coagulation with other particles (Darbyshire et al., 2019; Metcalf et al., 2013; Saturno et al., 2018b; Tasoglou et al., 2017; Wang et al., 2016), primary biomass burning aerosols have also been associated with high scattering efficiencies (Hand and Malm, 2007; Malm et al., 2005). Coating by non-absorbing material, such as Organics (Romshoo et al., 2021), has been shown to increase BC scattering by a factor of 3-24 depending on the size, morphology, aging stage, coating thickness and composition of the BC particles (He et al., 2015). Conversely, sulfate and water coating have also shown to increase elemental carbon particle diameter, playing a stronger role on its scattering efficiency, more than absorption (Cheng et al., 2008; Yu et al., 2010). Precisely quantifying distinct ARI for each chemical species, and especially decreasing uncertainties on the ones with high potential to both absorb

Formatted: Font color: Black

Formatted: Normal, Border: Top: (No border), Bottom: (N border), Left: (No border), Right: (No border), Between : (border), Tab stops: 3.13", Centered + 6.27", Right

and scatter radiation such as BC is critical to improve our understanding and prediction of the atmospheric system and improve climate models.

Chemical composition, processes, and sources of atmospheric aerosol particles in Amazonia have been widely studied during both the wet and dry seasons, in sites representing pristine conditions (Andreae et al., 2015; Cheng et al., 2015; Martin et al., 2010a) as well as strongly impacted by fires and urban pollution (Brito et al., 2014; Palm et al., 2018; Ponczek et al., 2021; Zaveri et al., 2022). Physical properties of radiation absorption and scattering have been described for the whole particles mass loading, regardless of the specific chemical groups (Artaxo et al., 2013; Nascimento et al., 2021; Palácios et al., 2020; Rizzo et al., 2013; de Sá et al., 2019; Sena et al., 2013). However, intensive optical properties of each aerosol species are still rare (Velazquez-Garcia et al., 2023), notably associated with OA origins (Ponczek et al., 2021) and with BC behaviour. Our study details the chemical properties of submicrometer aerosol particles in a forest site in central Amazonia during the dry season and their influence on radiation scattering and absorption. We applied positive matrix factorization (PMF) to the organic fraction, and associated mass extinction, absorption, and scattering efficiencies to different aerosol components via multi-linear regression (MLR) to improve our comprehension of their intrinsic properties, as well as estimate their role on ARI in Central Amazonia during the dry season.

2 Material and Methods

2.1 Sampling site

The measurements site is located in Central Amazonia, 60 km northwest of the city of Manaus, Brazil, in the Cuieiras biological reserve (2°35'39.24''S, 60°12'33.42''W~~), and referred to in this study as T0z~~). ~~(Martin et al., 2015; Whitehead et al., 2016).~~(Martin et al., 2015; Whitehead et al., 2016). The vegetation is characterized as *terra firme* (upland forest, not impacted by ~~seasonally flooded~~seasonal flooding), and the canopy is between 30 m and 35 m high ~~(Martin et al., 2010).~~(Martin et al., 2010a), 2010). As a result of steady northeasterly-easterly winds ~~(Andreae et al., 2015; Araújo et al., 2002)~~(Andreae et al., 2015; Araújo et al., 2002), only rarely the site is impacted by Manaus emissions (Chen et al., 2015). The ~~seasonality at the region of this site in central Amazonia has been previously defined as the~~ wet season in this region is typically from 1 December – 14 June, and the dry season from 15 June – 30 November (Andreae et al., 2015). During the wet season, air masses reaching the site pass over more than 1,500 km of undisturbed forest ~~(Andreae et al., 2015; Pöschl et al., 2010).~~(Pöschl et al., 2010). However, during the dry season, regional biomass burning pollution can be detected at the site ~~(Artaxo et al., 2013; Rizzo et al., 2013)~~(Artaxo et al., 2013; Rizzo et al., 2013), as well as aerosol plumes advected from African wildfires (Holanda et al., 2023). Our observations comprise from 1 August until 10 December 2013, sampling the atmosphere at 38.8 meters above ground level. The instrumentation was located inside an air-conditioned container at the base of the tower. A cyclone (50 % cut-off at 10 µm) was used at the entrance of the inlet. An automatic diffusion dryer ~~(Tuch et al., 2009)~~(Tuch et al., 2009) kept the relative humidity of the sampled air between 20% and 50%. Lodging for scientists/staff and a diesel generator were located

Formatted: English (United Kingdom)
Formatted: English (United Kingdom)
Formatted: English (United Kingdom)
Formatted: English (United Kingdom)
Formatted: English (United Kingdom)
Formatted: English (United Kingdom)
Formatted: English (United Kingdom)
Formatted: English (United Kingdom)
Formatted: English (United Kingdom)
Formatted: English (United Kingdom)
Formatted: English (United Kingdom)
Formatted: English (United Kingdom)
Formatted: English (United Kingdom)
Formatted: Font color: Black
Formatted: Normal, Border: Top: (No border), Bottom: (N border), Left: (No border), Right: (No border), Between : (border), Tab stops: 3.13", Centered + 6.27", Right

330m and 720m downwind (west) from the tower, respectively. The measurement tower has been shown to be practically unaffected by the generator (Whitehead et al., 2016). The year of this study (2013) was characterized by a historical minimum of fire detection over ~~the last~~ 20 years (Figure 1, ~~(F. G. Assis et al., 2019)~~(F. G. Assis et al., 2019)), providing an interesting outlook to assess the best scenarios for a dry season in recent times, and thus evaluate atmospheric composition within targets and goals for the ~~Amazon forest~~Amazonia rainforest preservation. The observation period here has been considered to fit entirely within dry-season atmospheric conditions. The previous transitional (wet-dry) period occurred in June-July ~~(Whitehead et al., 2016),~~(Whitehead et al., 2016), and the subsequent (dry-wet) soon after the end of our measurements.

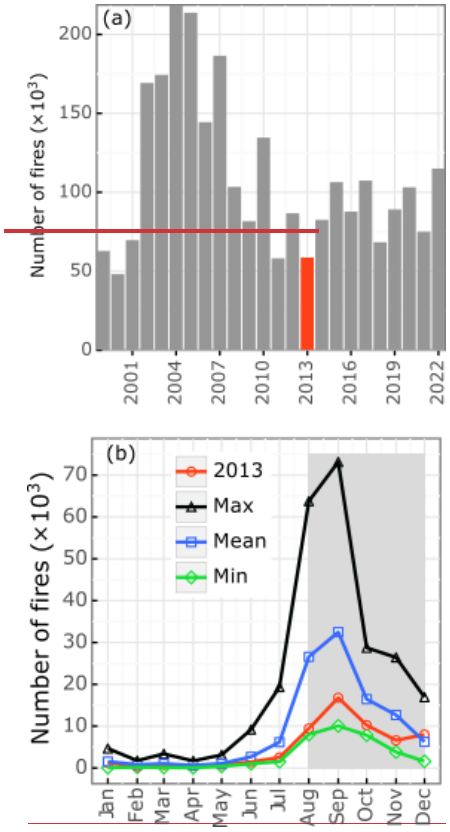

Formatted: English (United Kingdom)
Formatted: English (United Kingdom)
Formatted: English (United Kingdom)
Formatted: English (United Kingdom)
Formatted: Font color: Black
Formatted: Normal, Border: Top: (No border), Bottom: (N border), Left: (No border), Right: (No border), Between : (border), Tab stops: 3.13", Centered + 6.27", Right

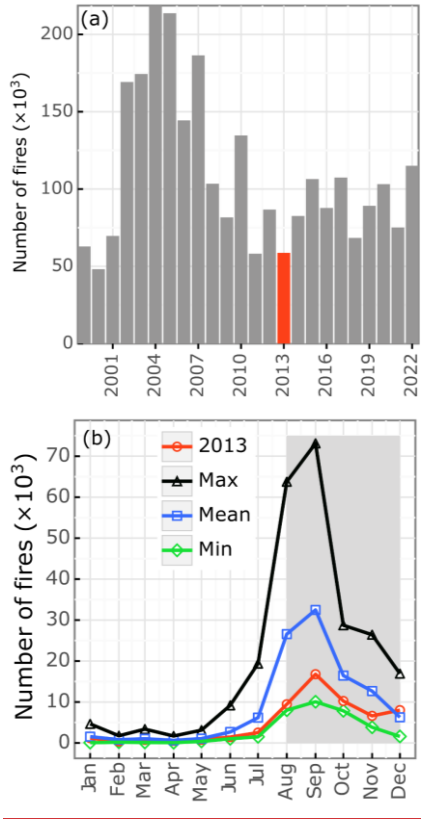

Figure 1: a) Number of fires in the Brazilian ~~Amazon forest~~Amazonia rainforest from 1999 to 2022, showing how 2013 (marked in red) ~~is~~has the lowest ~~in the past 20 years in terms of~~ total number of fires in 20 years, and b) mean (blue), maximum (black~~),~~) and minimum (green~~), and for 2013 (red~~) monthly fires between 1999-2022 in the ~~Amazon~~Amazonian Basin. The year of 2013 is marked in red, and it is evident how it was very close to the minimum (green) line. The gray area in b) marks the period of measurements in our study (01/Aug – 10/Dec) (Instituto Nacional de Pesquisas Espaciais, 2024).

2.2 Instrumentation

Non-refractory submicrometer aerosol composition was measured using a quadrupole Aerosol Chemical Speciation Monitor (ACSM, Aerodyne Research Inc) (Ng et al., 2011), which is a compact version of the Aerosol Mass Spectrometer (AMS).

Formatted: English (United Kingdom)
Formatted: English (United Kingdom)
Formatted: English (United Kingdom)
Formatted: English (United Kingdom)
Formatted: English (United Kingdom)
Formatted: English (United Kingdom)
Formatted: English (United Kingdom)
Formatted: English (United Kingdom)
Formatted: English (United Kingdom)
Formatted: Font color: Black
Formatted: Normal, Border: Top: (No border), Bottom: (N border), Left: (No border), Right: (No border), Between : (border), Tab stops: 3.13", Centered + 6.27", Right

Instrument calibration consisted of injecting monodispersed (300 nm) aerosol particles of ammonium nitrate (AN) and ammonium sulfate (AS~~). Aerosol particles were)~~, generated using an atomizer and subsequently dried, and size selected using a Differential Mobility Analyzer. A collection efficiency of 0.5 has been adopted (Middlebrook et al., 2012), yielding a very good agreement ~~in~~of particle mass considering measurements from different collocated instruments (S1). This method was successfully used in previous studies ~~(Brito et al., 2014; Sun et al., 2010)~~(Brito et al., 2014; Sun et al., 2010), and the value of 0.5 agrees with other studies in ~~the Amazon~~Amazonia during the dry season ~~(de Sá et al., 2019) and during the transition from wet to dry season (Ponczek et al., 2021).~~(Ponczek et al., 2021; de Sá et al., 2019). The measured ammonium (NH_4) mass concentrations were close to, or often lower than the detection limit of 0.28 ~~μm^{-3} (Pöhlker et al., 2018; Whitehead et al., 2016)~~μg m^{-3} (Pöhlker et al., 2018; Whitehead et al., 2016), and were therefore calculated based on nitrate (NO_3) and sulfate (SO_4) molar masses and their mass concentrations, assuming neutralization as in Equation 1:

$$NH_{4,\ predicted} = 18 \times \left(\frac{SO_4}{96} \times 2 + \frac{NO_3}{62}\right) \quad (1)$$

Furthermore, the SO_4 and NO_3 ions were used to estimate AS and AN (Equations 2 and 3) for the chemical-dependent optical properties analyses (Section 3.3), assumed here to be their most abundant form given the very low NH_4 levels:

$$AS = 132 \times \frac{SO_4}{96} \quad (2)$$

$$AN = 80 \times \frac{NO_3}{62} \quad (3)$$

Size-resolved particle number size distribution from 10 to 450 nm was measured with a Scanning Mobility Particle Sizer (SMPS, model 3081, TSI Inc.) coupled to a Condensation Particle Counter (CPC, model 3772, TSI Inc.) to provide equivalent mobility particle diameter for singly charged particles (D_{pg}, (Wiedensohler et al., 2012)~~.~~), Aerosol light scattering coefficient (σ_s) at 450 nm, 550 nm, and 700 nm (Anderson and Ogren, 1998) was measured using a Nephelometer (model 3563, TSI Inc.). Calibration was performed using CO_2 as the high-span gas and filtered air as the low-span gas. The averaging time applied was 60 minutes, and therefore the detection limits~~,~~ (defined as a signal-to-noise ratio of 2~~,~~) for scattering coefficients are 0.08, 0.03, and 0.05 Mm^{-1} for 450, 550, and 700 nm, respectively (Anderson and Ogren, 1998). ~~Since a PM10 inlet was used, the "no-cut" factors were used for the truncation corrections (Anderson and Ogren, 1998). Scattering coefficients at 637 nm were calculated from interpolation, assuming a power-law spectral dependency. A~~Since a PM10 inlet was used, the "no-cut" factors were used for the truncation corrections. We used a Multi Angle Absorption Photometer (MAAP, model 5012, Thermo Electron Group, Waltham, USA) (Müller et al., 2011) ~~measured~~to measure aerosol light absorption coefficient (σ_a) at 637 nm, and ~~was used~~ to estimate equivalent Black Carbon (eBC) concentration, assuming an absorption cross-section value of 6.6 m^2 g^{-1}. Considering the conditions of the experiment, the MAAP detection limit for σ_a was of 0.13 Mm^{-1} (Petzold et al., 2005).

Formatted: English (United Kingdom)
Formatted: English (United Kingdom)
Formatted: English (United Kingdom)
Formatted: English (United Kingdom)
Formatted: Font: Times New Roman, English (United Kingdom)
Formatted: Font: Times New Roman, English (United Kingdom)
Formatted: Font: Times New Roman, English (United Kingdom), Pattern: Clear, Highlight
Formatted: English (United Kingdom)
Formatted: English (United Kingdom)
Formatted: English (United Kingdom)
Formatted: English (United Kingdom)
Formatted: English (United Kingdom)
Field Code Changed
Formatted: English (United Kingdom)
Formatted: English (United Kingdom)
Formatted: English (United Kingdom)
Formatted: English (United Kingdom)
Formatted: Font: Gungsuh, English (United Kingdom)
Formatted: English (United Kingdom)
Formatted: English (United Kingdom)
Formatted: English (United Kingdom)
Formatted: English (United Kingdom)
Formatted: English (United Kingdom)
Formatted: English (United Kingdom)
Formatted: English (United Kingdom)
Formatted: Font: Gungsuh, English (United Kingdom)
Formatted: English (United Kingdom)
Formatted: Font color: Black
Formatted: Normal, Border: Top: (No border), Bottom: (N border), Left: (No border), Right: (No border), Between : (border), Tab stops: 3.13", Centered + 6.27", Right

Episodes of possible contamination from the city of Manaus and from the diesel generator were removed by filtering the datapoints when either the wind direction was between 270-340° (from our local wind direction measurements) or when the calculated backtrajectories from the Hysplit model (Draxler and Hess, 1998) passed over Manaus coordinates, as in (Whitehead et al., 2016) (Supplement S2).

2.3 Optical properties

~~Single Scattering Albedo (SSA, Equation 4) is a measure of the ratio of σ_s to the total radiation extinction coefficient ($\sigma_e = \sigma_s + \sigma_a$) by aerosol particles (Rizzo et al., 2013). Since the MAAP instrument only measures the σ_a at 637 nm wavelength, the σ_e was calculated only for this wavelength using σ_s at 637 nm from the nephelometer, estimated using the scattering Angstrom exponent (α_s, Equation 5).~~

~~$$SSA = \frac{\sigma_s}{\sigma_s + \sigma_a} \quad (4)$$~~

~~The α_s is a measure of the dependence of radiation scattering on the light wavelength (λ), and it is an indication of particle size (Rizzo et al., 2013; Saturno et al., 2018b; Schuster et al., 2006):~~

~~$$\ln \sigma_s = -\alpha_s \ln \lambda + \ln (constant) \quad (5)$$~~

Scattering coefficients at 637 nm were calculated from interpolation using the scattering Angström exponent (α_s, Equation 4), assuming a power-law spectral dependency. The α_s is a measure of the dependence of radiation scattering on the light wavelength (λ), and it is an indication of particle size (Rizzo et al., 2013; Saturno et al., 2018b; Schuster et al., 2006):

$$ln\ \sigma_s = -\alpha_s\ ln\ \lambda + ln\ (constant) \quad (4)$$

Single Scattering Albedo (SSA, Equation 5) is a measure of the ratio of σ_s to the total radiation extinction coefficient ($\sigma_e = \sigma_s + \sigma_a$) by aerosol particles (Rizzo et al., 2013). Since the MAAP instrument only measures the σ_a at a wavelength of 637 nm, the σ_e was calculated using σ_s at 637 nm interpolated from the nephelometer.

$$SSA = \frac{\sigma_s}{\sigma_s + \sigma_a} \quad (5)$$

After rain events and other moments when the atmosphere is very clean, ~~both α_s for σ_e values~~all the optical parameters are ~~very low~~close to zero, and therefore the ratio between them ~~(SSA, Equation 4)~~ becomes unrealistically high. We therefore calculated SSA ~~for α_s for~~only when σ_s and $\sigma_e > 1\ Mm^{-1}$.

Formatted: English (United Kingdom)

Formatted: Font color: Black

Formatted: Normal, Border: Top: (No border), Bottom: (No border), Left: (No border), Right: (No border), Between : (No border), Tab stops: 3.13", Centered + 6.27", Right

2.4 Statistical Analyses

2.4.1 Positive Matrix Factorization (PMF)

~~The PMF (Positive Matrix Factorization) was used on the submicrometer non-refractory organic mass spectra in order to group m/z ratios with similar temporal variability, supporting the identification of sources and processes that formed and transformed atmospheric particles. A detailed description of the PMF can be found in (Paatero & Tapper, 1994; Ulbrich et al., 2009), and it is an established methodology for aerosol source apportionment (Zhang et al., 2011). The model can be represented by the following Equation. (6):~~

We used Positive Matrix Factorization (PMF) in order to group the submicrometer non-refractory organic mass spectra (m/z ratios) with similar temporal variability, supporting the identification of sources and processes that formed and transformed atmospheric particles (Paatero and Tapper, 1994; Ulbrich et al., 2009; Zhang et al., 2011). The model can be represented by the following Equation. (6):

$$X_{(m\times n)} = \sum = \sum G_{(m\times p)} \cdot F_{(p\times n)} + E \quad (6)$$

Where **X** is the input matrix of *n* (elements – m/z ratios) lines and *m* (number of samples) columns ~~(Ulbrich et al., 2009).~~ (Ulbrich et al., 2009). In this study, the **X** matrix had 2901 lines (1-hour averages for more than 4 months of measurements) and 70 columns (m/z ratios). The receptor model aims to determine the number of *p* factors, representing sources or processes, their chemical composition, and the relative contribution of each factor. **G** is a matrix in which columns are the time series of the factors. **F** is a matrix in which lines are the profiles of the factors (mass spectra). **E** represents the residuals, the part of the data that was not ~~modeled~~modelled by any factor *p*. We used an IGOR™-based interface to apply the PMF analysis (Ulbrich et al., 2009). The PMF ions were normalized to the organics concentration.

2.4.2 Multilinear Regression (MLR)

~~We used a Multilinear Regression (MLR) model to estimate the contribution of each aerosol chemical component to scattering, absorption, and extinction coefficients, deriving the corresponding efficiencies (MSE, MAE, and MEE, respectively). The σ_s and σ_a were the dependent variables (response) and the species/factors were the independent (predictor) variables.~~

We used a Multilinear Regression (MLR) model to estimate the contribution of each aerosol chemical component to scattering, absorption, and extinction coefficients, deriving the corresponding efficiencies (MSE, MAE, and MEE, respectively) (Yu et al., 2010). The scattering (σ_s) and extinction (σ_e) coefficients (Mm^{-1}) were the dependent variables (response) and the ACSM species/PMF factors were the independent (predictor) variables.

A generalization of the mass efficiency (ME) calculation is presented in Equation 7:

$$ME = \sum_i a_i x_i + r \quad (7)$$

Formatted: English (United Kingdom)
Formatted: English (United Kingdom)
Formatted: English (United Kingdom)
Formatted: English (United Kingdom)
Formatted: English (United Kingdom)
Formatted: English (United Kingdom)
Formatted: English (United Kingdom)
Formatted: English (United Kingdom)
Formatted: English (United Kingdom)
Formatted: English (United Kingdom)
Formatted: English (United Kingdom)
Formatted: English (United Kingdom)
Formatted: English (United Kingdom)
Formatted: English (United Kingdom)
Formatted: English (United Kingdom)
Formatted: Font color: Black
Formatted: Normal, Border: Top: (No border), Bottom: (N border), Left: (No border), Right: (No border), Between : (border), Tab stops: 3.13", Centered + 6.27", Right

Where ME can be MSE, MAE or MEE; x is the chemical species mass concentration; a_i is the efficiency of each component, and r are the residuals. We used NNLS (Non-Negative Least Squares) from Python package Scipy version 1.5.2 ~~(Virtanen et al., 2020). To constrain the model to produce results with physical meaning, the coefficients a_i were constrained to be positive, as in (Velazquez-Garcia et al., 2023). Since eBC is assumed to be the only absorbing component measured in this study with the MAAP, a MLR could not be applied,~~(Virtanen et al., 2020). To constrain the model to produce results with physical meaning, the coefficients a_i were constrained to be positive, as in (Velazquez-Garcia et al., 2023). Since eBC is assumed to be the only absorbing component measured in this study with the MAAP, a MLR could not be applied for $\sigma_{a,}$ and the MAE was considered to be equivalent to the cross-section value (6.6 m^{-2} g^{-1}, Section 2.2).

3 Results and Discussion

3.1 Aerosol chemical composition

The concentrations of organics and inorganics aerosols follow similar variation patterns during the measurement period (Figure 2a). This can be an indication that the total mass loading consists of well-mixed biomass burning and secondary aerosols, associated with large and regional-scale processes (Darbyshire et al., 2019). The total submicrometer (PM1 = Organics + NO_3 + NH_4 + SO_4 + eBC) mean mass concentration during the observation period was 6.3±3.3 µg m^{-3} (Table 1, Figure ~~1a~~2a). This represents about half of what was measured during the dry season of the following year (2014, with much more fires, Figure 1) at a nearby site ~~(ATTO tower, Amazon Tall Tower Observatory),~~ with similar conditions ~~(Central~~in central Amazonia~~, isolated from major biomass burning focus or Manaus urban plume) (10.5 µg m^{-3}~~ (ATTO, (de Sá et al., 2019)~~) and regions directly impacted by fires during the dry season (12.4-13.7 µg m^{-3} (Brito et al., 2014; Ponczek et al., 2021)).~~

~~The PM1 aerosol composition was dominated by the organic fraction, representing a mass fraction of 77±5% (Table 1, Figure 2b). This is very similar to the wet season and wet to dry season transition in the same site (> 80% (Artaxo et al., 2013; Chen et al., 2015; Whitehead et al., 2016)), but high compared to other continental urban areas, such as across Europe (~30-50%,~~ and regions directly impacted by fires during the dry season (Brito et al., 2014; Ponczek et al., 2021). The PM1 aerosol composition was dominated by the organic fraction (77±5%, Table 1, Figure 2b), similar to what was found in the same site in wetter conditions (Artaxo et al., 2013; Chen et al., 2015; Whitehead et al., 2016), but lower than what was found in a region highly impacted by biomass burning in southwestern Amazonia (Brito et al., 2014). In continental urban areas, such as across Europe, the organic particles represented a much lower fraction of the total particles mass, (Chen et al., 2022)~~) and lower than the strongly impacted by biomass burning region in Southwestern Amazonia (90%, (Brito et al., 2014). Sulfate is the main soluble inorganic component of the aerosol mass fraction in the Amazon~~. Sulfate is the main soluble inorganic component of the aerosol mass fraction in Amazonia, both during the wet and dry seasons ~~(Fuzzi et al., 2007; Yamasoe et al., 2000)~~(Fuzzi et al., 2007; Yamasoe et al., 2000). In our study, the mean SO_4 mass fraction was 9±3% (Table 1, Figure 2b), which is

Formatted: English (United Kingdom)
Formatted: English (United Kingdom)
Formatted: English (United Kingdom)
Formatted: English (United Kingdom)
Formatted: English (United Kingdom)
Formatted: English (United Kingdom)
Formatted: English (United Kingdom)
Formatted: English (United Kingdom)
Formatted: English (United Kingdom)
Formatted: Font color: Black
Formatted: Normal, Border: Top: (No border), Bottom: (No border), Left: (No border), Right: (No border), Between : (No border), Tab stops: 3.13", Centered + 6.27", Right

comparable to the ATTO site (Andreae et al., 2015). However, in Southwestern Amazonia, in areas impacted by fresh biomass burning, the average SO_4 mass fraction was significantly lower (2-3% ~~(Brito et al., 2014; Ponczek et al., 2021)).~~(Brito et al., 2014; Ponczek et al., 2021)).

The eBC mass fraction was 6±2% (Table 1, Figure 2b), which is half ~~than~~of the fraction observed in the wet season at the same site ~~(11%), despite the much lower total submicrometer aerosol mass loading~~ (Chen et al., 2015)~~.~~, despite the much lower total submicrometer aerosol mass loading. Occasional urban pollution from Manaus, long-range transport from Africa, and potential artifacts combined with much lower overall aerosol loading are possible causes for this ~~relatively~~ higher eBC mass fraction found in the wet season (Chen et al., 2015)~~. In Southwestern Amazonia, during the transition from dry to wet season, the contribution of eBC to PM1 reached 15% (Ponczek et al., 2021). Nitrate had a minor contribution during our observations (3±1%), with concentration levels comparable to the ATTO site (Pöhlker et al., 2018), as well as Southwestern Amazonia (Brito et al., 2014; Ponczek et al., 2021)). The concentrations of organics and inorganics follow similar patterns during the measurement period (Figure 2a). This can be an indication that the total mass loading consists of well-mixed biomass burning and secondary aerosols, associated with large and regional-scale processes (Darbyshire et al., 2019)~~. In Southwestern Amazonia, highly impacted by fresh biomass burning, the contribution of eBC to PM1 reached 15% (Ponczek et al., 2021). Nitrate had a minor contribution during our observations (3±1%), with concentration levels comparable to the ATTO site (Pöhlker et al., 2018), as well as Southwestern Amazonia (Brito et al., 2014; Ponczek et al., 2021).

Formatted: English (United Kingdom)

Formatted: English (United Kingdom)

Formatted: English (United Kingdom)

Formatted: English (United Kingdom)

Formatted: English (United Kingdom)

Formatted: English (United Kingdom)

Formatted: English (United Kingdom)

Formatted: Font color: Black

Formatted: Normal, Border: Top: (No border), Bottom: (N border), Left: (No border), Right: (No border), Between : (border), Tab stops: 3.13", Centered + 6.27", Right

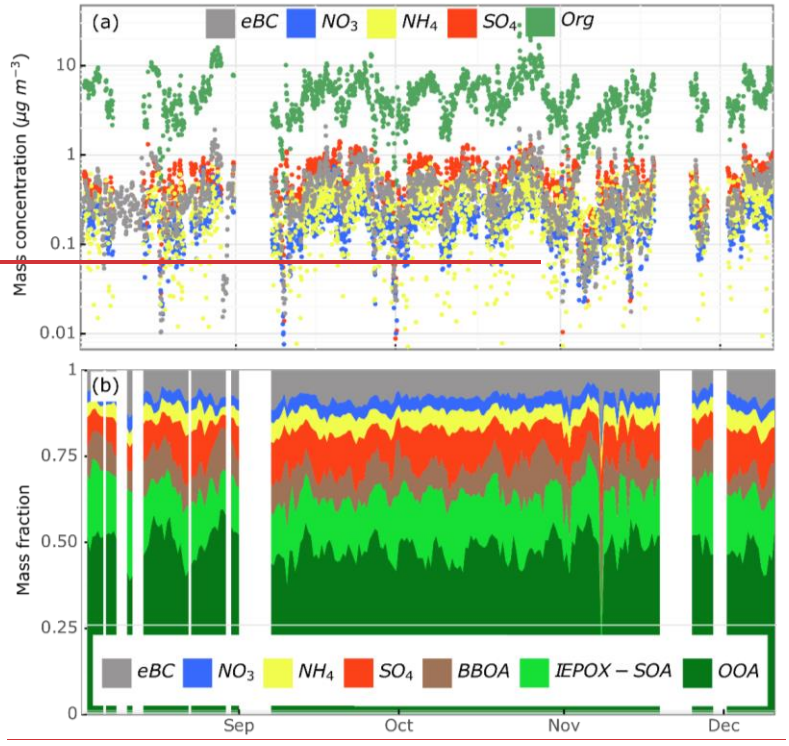

Formatted: Font color: Black

Formatted: Normal, Border: Top: (No border), Bottom: (No border), Left: (No border), Right: (No border), Between : (No border), Tab stops: 3.13", Centered + 6.27", Right

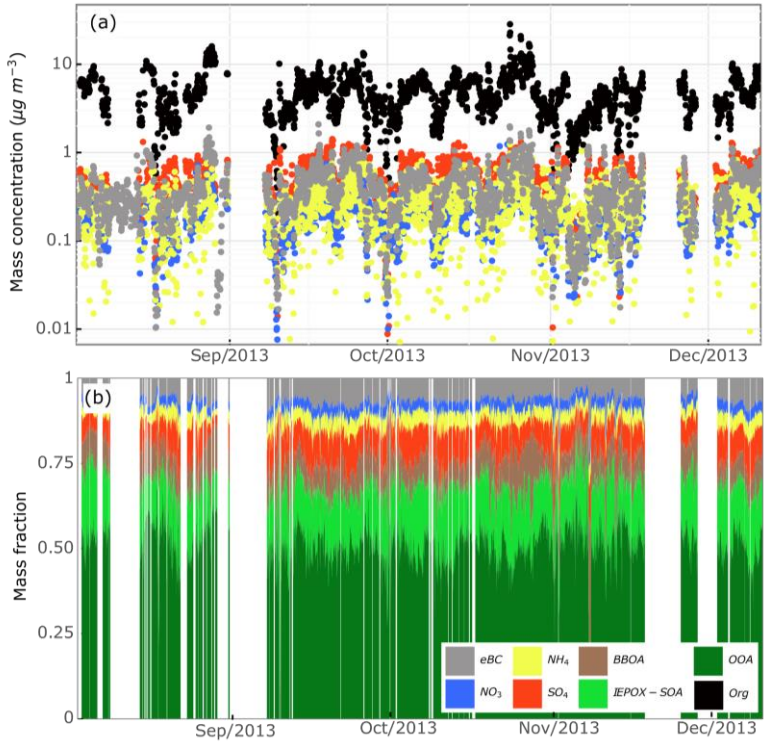

Figure 2: Non-refractory submicrometer aerosol species and eBC mass (a) concentrations and (b) fractions ~~at T0z~~. In (a) the vertical axis is the logarithm scale to facilitate the visualization of different species. ~~In (a), data is shown in the original time stamp of 1 hour, while in (b) it was averaged to 12 hours in order to facilitate visualization.~~

The PMF analysis yielded 4 ~~factors, although 2~~ statistical factors, although 2 of them were closely related to the Oxygenated Organic Aerosol (OOA) fraction~~, and the~~. Their mass spectra, ~~diurnal~~daily profile, and time series of these factors did not present enough differences to justify their separation (Supplements S3 and S4). Therefore, these 2 factors were manually summed in order to generate a 3 factors solution, which was different from the factors found in the 3 factors solution presented by the PMF. In (Ulbrich et al., 2009), the authors describe how one PMF resulting statistical factor can split into various other factors which, after added, represent the real factor. The recombination often considers similarities between the statistical factors in the mass spectra, ~~diurnal~~daily profile and time series (Carbone et al., 2013). In our study, the identification of the factors was further confirmed with the correlation between the PMF statistical factors and the inorganic aerosols, with the eBC

Formatted: English (United Kingdom)
Formatted: English (United Kingdom)
Formatted: English (United Kingdom)
Formatted: English (United Kingdom)
Formatted: English (United Kingdom)
Formatted: English (United Kingdom)
Formatted: English (United Kingdom)
Formatted: English (United Kingdom)
Formatted: English (United Kingdom)
Field Code Changed
Formatted: English (United Kingdom)
Formatted: English (United Kingdom)
Formatted: English (United Kingdom)
Field Code Changed
Formatted: Font color: Black
Formatted: Normal, Border: Top: (No border), Bottom: (N border), Left: (No border), Right: (No border), Between : (border), Tab stops: 3.13", Centered + 6.27", Right

(Supplement S4) and ~~diurnal~~daily profile analyses. The 3 factors were identified as BBOA (Biomass Burning Organic Aerosol), OOA (Oxygenated Organic Aerosol) and IEPOX-SOA (Isoprene derived Epoxydiol–Secondary Organic Aerosol), and they represent together 99% of the measured submicrometer organic aerosol mass, with 1% of residuals. The correlation between BBOA and NO_3 and SO_4 is comparable with findings in Southwestern Amazonia (Brito et al., 2014).

Table 1 - Dry season (01/Aug – 10/Dec) mean mass concentration (μ m^{-3}), standard deviations, and percentile range (10-90, in parenthesis) of the species measured by the ACSM and MAAP (eBC).

	Mass concentration (μg m^{-3})	Mass fraction
Total PM1	6.3±3.3 (2.7-10.3)	100%
Organics	4.9±2.7 (2.1-7.9)	77±5%
BBOA	*0.6±0.6 (0.2-1.1)*	9±5%
IEPOX-SOA	1.0±*0.5 (0.4-1.7)*	*17*±5%
OOA	3.2±*1.5 (1.3-5.5)*	*51±6%*
NO_3	0.2±0.1 (0.1-0.3)	3±1%
NH_4	0.3±0.1 (0.0-0.5)	4±1%
SO_4	0.5±0.3 (0.2-0.9)	9±3%
eBC	0.4±0.3 (0.1-0.7)	6±2%

The ~~largest contribution~~dominant PMF-derived statistical factor in our study was OOA, which contributed to 51±6% of the PM1 (Table 1), and 65% of the organic mass. ~~It presented the largest m/z 44 fraction (Figure 3), and therefore, this is the factor~~ This agrees with ~~the highest estimated O:C ratio (Chen et al., 2015). The high oxidation level indicates highly aged particles and may lose some of their original chemical signatures, in terms of elementary ratios, during the aging process (Jimenez et al., 2009). The m/z 44 is formed mainly by the fragment CO_2^+, typical of the thermal decarboxylation of the organic acids groups (Alfarra et al., 2004).~~previous studies showing that highly processed SOA are a ~~The more aged the aerosols, the more chemically similar they become, which makes the task of separating them into different factors with distinctive characteristi cs very difficult. Therefore, the OOA factor probably groups aerosol particles from different sources, and their common characteristic is that they are probably originating relatively distant from the sampling site.~~ ~~This factor is a~~ major component of ~~basin-wide haze observed during biomass burning season, associated with the transport from eastern Amazonia into~~the atmospheric particles in remote ~~central~~ regions ~~at the center~~ of ~~the basin~~Amazonia (Darbyshire et al., 2019). This factor has the highest estimated O:C ratio, which is evident in the observed m/z 44 fraction (Figure 3, note the different scales). The high oxidation level indicates highly aged particles and may lose some of their original chemical signatures, in terms of elementary ratios, during the aging process (Jimenez et al., 2009). The m/z 44 signal predominantly arises from the CO_2^+ ion fragment, which is typically generated by thermal decarboxylation of carboxylic acid functional groups in organic aerosols (Alfarra et al., 2004). Therefore, m/z 44 serves as a valuable marker for the extent of aerosol oxidation and the presence of oxygenated

Formatted: English (United Kingdom)
Formatted Table
Formatted: English (United Kingdom)
Formatted: Portuguese (Brazil)
Formatted: English (United Kingdom)
Formatted: Font: 10 pt, Portuguese (Brazil)
Formatted: English (United Kingdom)
Formatted: English (United Kingdom)
Formatted: English (United Kingdom)
Formatted: English (United Kingdom)
Formatted: English (United Kingdom)
Formatted: English (United Kingdom)
Formatted: English (United Kingdom)
Formatted: English (United Kingdom)
Formatted: English (United Kingdom)
Formatted: English (United Kingdom)
Formatted: English (United Kingdom)
Formatted: English (United Kingdom)
Formatted: English (United Kingdom)
Formatted: Font color: Black
Formatted: Normal, Border: Top: (No border), Bottom: (N border), Left: (No border), Right: (No border), Between : (border), Tab stops: 3.13", Centered + 6.27", Right

organic compounds, providing insight into aerosol aging and secondary organic aerosol formation processes. The more aged the aerosols, the more chemically similar they become, which makes the task of separating them into different factors with distinctive characteristics very difficult. Therefore, the OOA factor probably groups aerosol particles from different sources, and their common characteristic is that they are probably originating relatively distant from the sampling site.

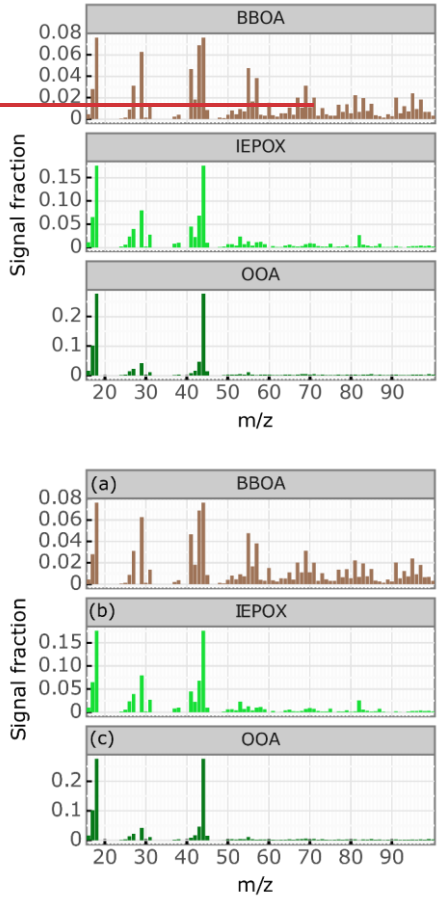

Figure 3: PMF Mass spectra composition of each statistical factor and its relative contribution to the total submicrometer organic aerosol mass. It is possible to observe typical tracer ions such as m/z 60 and m/z 73 that characterize the BBOA factor, and also the

Formatted: English (United Kingdom)

Formatted: English (United Kingdom)

Formatted: Font color: Black

Formatted: Normal, Border: Top: (No border), Bottom: (N border), Left: (No border), Right: (No border), Between : (border), Tab stops: 3.13", Centered + 6.27", Right

m/z 82 in the IEPOX-SOA factor. The scale of the Y axis is different in order to facilitate visualisation of m/z signal fractions mainly of (a) and (b).

The production of IEPOX-SOA generally leads to the production of markers in the atmosphere, such as the 2-methylthetrol and the 3-methylfuran (m/z 82, $C_5H_6O^+$). These markers may not originally exist in the IEPOX-SOA molecule due to their extremely high volatility, but they can be formed during the decomposition of some IEPOX-SOA species, such as 3-methyltetrahydrofuran-3,4-diols (3-MeTHF-3,4-diols) (Lin et al., 2012).$^+$) (Lin et al., 2012). The organic fraction in the m/z 82 is therefore important for the identification of the IEPOX-SOA factor (Figure 3b, despite its low contribution to the submicrometer organic aerosol mass fraction (usually below 4%). Beyond that, most% of submicrometer organic aerosol). Most of the other m/z are common to other factors, making the m/z 82 distinctive of the IEPOX-SOA, which can also be identified by the m/z 53 ($C_4H_5^+$) and m/z 75 ($C_3H_7O_2^+$) (Allan et al., 2014; Lin et al., 2012; Xu et al., 2015a). The lifetime of IEPOX-SOA in the boundary layer is estimated to be about 2 weeks (Hu et al., 2016). The IEPOX-SOA mean mass concentration in our study was 1.0±0.5 μg m^{-3} (Table 1, Figure 4). Previous studies reported 0.26 μg m^{-3} during the wet season(Figure 3b) (Allan et al., 2004; Lin et al., 2012; Xu et al., 2015). IEPOX-SOA mean mass concentration in our study was 1.0±0.5 μg m^{-3} (Table 1). Previous studies reported 0.26 μg m^{-3} during the wet season at the same site (Chen et al., 2015), while downwind of Manaus it was around 0.5 μg m^{-3} during background conditions, and 0.1 μg m^{-3} during polluted conditions (de Sá et al., 2017)(de Sá et al., 2017). It is important to note that at T0z, while While the organic particle loading typically increases by an order of magnitude from the wet to the dry season (Artaxo et al., 2013), we estimated that IEPOX-SOA increases about a factor ~3. The relative contribution of IEPOX-SOA to organics during the wet season was estimated to be 34%, in contrast to the 17% found in this study (Table 1), whichIEPOX-SOA increases by about a factor ~3 (Table 1 and (Chen et al., 2015), while its relative contribution to the organic aerosols drops by half (from 34% (Chen et al., 2015) to 17%, Table 1). This is likely the result of a complex balance between increased isoprene emissions (Yáñez-Serrano et al., 2015)(Yáñez-Serrano et al., 2015), sulfate abundance and increased pollution levels (including NO_x from forest fires, and biomass-burning related aerosol particles). The relative contribution of IEPOX-SOA to the total PM1 mass was relatively constant during the whole measurement period (Figure 2b), as well as most of the other species (with the exception of some episodes). This indicates that an atmospheric dynamics of rain/dilution controlling the chemical composition could be more important than the influence of local sources of particles, confirming the regional haze hypothesis raised by (Darbyshire et al., 2019).

The correlation (Pearson coefficient = 0.7) observed between the IEPOX-SOA factor and AS (Supplement S4.1) is similar to the correlation measured in regions affected by urban pollution in the Amazon, Africa and USA (R^2 = 0.37-0.48 (Brito et al., 2018; Budisulistiorini et al., 2013; de Sá et al., 2017)). Sulfate is the main aqueous phase particle in which isoprene products use to condense on (Budisulistiorini et al., 2013; Kroll et al., 2006; Lin et al., 2012; Marais et al., 2016; Surratt et al., 2010; Xu et al., 2015b), and therefore a positive and moderate-high correlation is expected. eBC presents a similar correlation with IEPOX-SOA as AS (Supplement S4), but the correlation is even higher with the other PMF statistical factors, especially OOA

Formatted: English (United Kingdom)
Formatted: English (United Kingdom)
Formatted: English (United Kingdom)
Formatted: English (United Kingdom)
Formatted: English (United Kingdom)
Formatted: English (United Kingdom)
Formatted: English (United Kingdom)
Formatted: English (United Kingdom)
Formatted: English (United Kingdom)
Formatted: Font color: Black
Formatted: Normal, Border: Top: (No border), Bottom: (No border), Left: (No border), Right: (No border), Between : (No border), Tab stops: 3.13", Centered + 6.27", Right

~~(Pearson coefficient = 0.85, Supplement S4). Since OOA corresponds to more than half of PM1 (Table 1), this high correlation indicates that most of the submicrometer aerosols measured during the dry season in Central Amazonia are, in general, influenced by biomass burning emissions, since eBC is an important combustion tracer. However, the fact that the eBC correlation is higher with the OOA factor than with BBOA (which constitutes only 9% of PM1, Table 1, Supplement S4) indicates that long-range transport of aged and internally well mixed biomass burning plumes plays a more important role than nearby fire sources~~ The correlation (Pearson coefficient = 0.7) observed between the IEPOX-SOA factor and AS (Supplement S4.1) is similar to the correlation measured in regions affected by urban pollution in Amazonia, Africa and USA (Brito et al., 2018; Budisulistiorini et al., 2013; de Sá et al., 2017). Sulfate is the main aqueous phase particle in which isoprene products condense on, and therefore a positive and moderate-high correlation is expected (Budisulistiorini et al., 2013; Kroll et al., 2006; Lin et al., 2012; Marais et al., 2016; Surratt et al., 2010; Xu et al., 2015). eBC presents a similar correlation with IEPOX-SOA as AS (Supplement S4), but the correlation is even higher with the other PMF factors, especially OOA (Pearson coefficient = 0.85, Supplement S4). This suggests that a significant fraction of the aged submicrometer aerosols measured during the dry season in Central Amazonia is largely influenced by biomass burning emissions, in combination with other combustion sources such as sporadic urban plumes transported from Manaus. In addition, co-variability between aerosol species is expected due to strong washout events that, although less frequent, can still occur during the dry season and impact multiple aerosol components simultaneously. The fact that the eBC correlation is higher with the OOA factor than with BBOA (which constitutes only 9% of PM1, Table 1, Supplement S4) indicates that long-range transport of aged and internally well mixed biomass burning plumes plays a more important role than nearby sources (Darbyshire et al., 2019).

The BBOA factor can be identified by the presence of the m/z 60 and m/z 73 (Figure ~~3~~3a), which are dominated by the $C_2H_4O_2^+$ and the $C_3H_5O_2^+$ fragments. These fragments are originated from levoglucosan and other similar anhydro-sugars (such as manosan and galactosan). Levoglucosan (1,6-*â*-D-anhydroglucopyranose, $C_6H_{10}O_5$) is known as a biomarker of biomass burning emissions due to its production from the pyrolysis of carbohydrates as cellulose ~~(Alfarra et al., 2007; Artaxo et al., 2013; Chen et al., 2009; Lee et al., 2010)~~(Alfarra et al., 2007; Artaxo et al., 2013; Chen et al., 2009; Lee et al., 2010). The signal fraction of m/z 60 for the BBOA factor in our study was 1.5%, which is 5 times higher than the 0.3% threshold typically used as an appropriate background fraction for biomass burning (Cubison et al., 2011). OOA presented a m/z 60 signal fraction of 0.2%, while IEPOX-SOA presented a negligible signal.

~~The BBOA diurnal profile is different from that of the other PMF factors (Figure 4). While the OOA and IEPOX-SOA mass concentrations increase during the daytime due to photochemical oxidation processes, the BBOA mass concentration is fairly constant (Figure 4). Since the BBOA is a biomass-burning indicator, it is composed of mostly primary particles, so its concentration does not depend on photochemical activity. This pattern is different than the stark decrease in mass concentrations of fresh biomass burning particles during daytime, observed~~The daily profile of BBOA differs significantly from other factors (Figure 4). While OOA and IEPOX-SOA mass loadings increase during the day, likely due to photochemically driven oxidation processes, BBOA remains relatively constant throughout the day, despite the daytime dilution effect of a rising boundary layer (Andreae et al., 2015). Interestingly, this pattern contrasts with the pronounced

Formatted: English (United Kingdom)

Formatted: English (United Kingdom)

Formatted: English (United Kingdom)

Formatted: Font: Times New Roman, English (United Kingdom)

Formatted: English (United Kingdom)

Formatted: English (United Kingdom)

Formatted: Font color: Black

Formatted: Normal, Border: Top: (No border), Bottom: (No border), Left: (No border), Right: (No border), Between : (No border), Tab stops: 3.13", Centered + 6.27", Right

daytime decrease in fresh biomass-burning aerosol concentrations reported in southwestern Amazonia (Brito et al., 2014), where ~~there were constant local sources of fires and the diurnal cycle was mostly determined by the boundary layer increasing and diluting the particles in a bigger area during daytime (Andreae et al., 2015). The lack of a clear diurnal pattern in our study for BBOA seems to confirm the regional origin of the aerosol particles, likely transported from distant biomass burning sources in the eastern parts of the basin, and long-range transport with complex~~local fire emissions were more prevalent. The absence of a clear diurnal cycle for BBOA in our study corroborates a regional, rather than local, origin—likely from biomass-burning sources located in the eastern Amazon. The flat variability of this primary factor reflects transport over long distances and the influence of complex vertical mixing, including interactions between residual and nocturnal layers (Darbyshire et al., 2019). ~~An additional confirmation of the long-range transport~~

Further supporting this hypothesis, is the relatively flat ~~pattern of the eBC diel~~daily cycle of eBC, although ~~there is a small but noticeable~~ slight daytime increase ~~in the eBC diurnal mass concentration during daytime~~ is observed (Figure 4), ~~which may indicate some~~ possibly due to lensing ~~effect due to the increase in the particle coating~~effects as particles acquire coatings during transport (Denjean et al., 2020). ~~While the diel cycle of the~~Unlike eBC, NH_4 and NO_3 show ~~practically no~~minimal diurnal variation, ~~the~~while SO_4 ~~indicates the influence of~~exhibits a daytime increase, consistent with secondary production via photochemical ~~processes (Figure 4)~~reactions from biogenic sources, or atmospheric transport processes. The ~~higher~~rise in the boundary layer ~~in~~during the afternoon ~~(Fisch et al., 2004) may favor the downward transport of long-distance particles~~ (Fisch et al., 2004) may facilitate the entrainment of particles from above the boundary layer (Darbyshire et al., 2019). ~~An additional possible explanation for this observed increase in SO_4 during the afternoon is biogenic sources of SO_4 precursors.~~

~~As the OOA and the IEPOX-SOA factors represent together around 68% of the total mass fractions of the submicron particles during our study, and conversely, eBC and BBOA represent only 15%, the importance of the atmospheric photochemical activity in Central Amazonia becomes evident. Well-preserved parts of the Amazon are strongly affected by the regional transport of well-processed biomass burning plumes, overwhelming the local biogenic processes that usually modulate the diurnal behavior of secondary aerosol development (Artaxo et al., 2013; Darbyshire et al., 2019).~~

Formatted: English (United Kingdom)

Formatted: English (United Kingdom)

Formatted: English (United Kingdom)

Formatted: English (United Kingdom)

Formatted: English (United Kingdom)

Formatted: English (United Kingdom)

Formatted: English (United Kingdom)

Formatted: English (United Kingdom)

Formatted: English (United Kingdom)

Formatted: English (United Kingdom)

Formatted: English (United Kingdom), Not Superscript/ Subscript

Formatted: English (United Kingdom)

Formatted: English (United Kingdom)

Formatted: English (United Kingdom)

Formatted: English (United Kingdom)

Formatted: English (United Kingdom)

Formatted: English (United Kingdom)

Formatted: English (United Kingdom)

Formatted: English (United Kingdom)

Formatted: English (United Kingdom)

Formatted: Font color: Black

Formatted: Normal, Border: Top: (No border), Bottom: (N border), Left: (No border), Right: (No border), Between : (border), Tab stops: 3.13", Centered + 6.27", Right

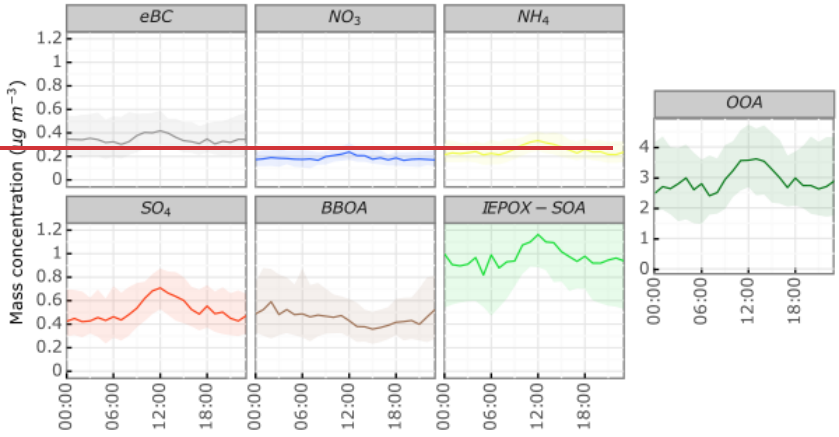

As the OOA and the IEPOX-SOA factors represent together around 68% of the total mass fractions of the submicron particles during our study (Table 1), and conversely, eBC and BBOA represent only 15%, the importance of the atmospheric photochemical activity in Central Amazonia becomes evident. Well-preserved parts of Amazonia are strongly affected by the regional transport of well-processed biomass burning plumes, overwhelming the local biogenic processes that usually modulate the daily behavior of secondary aerosol development (Artaxo et al., 2013; Darbyshire et al., 2019).

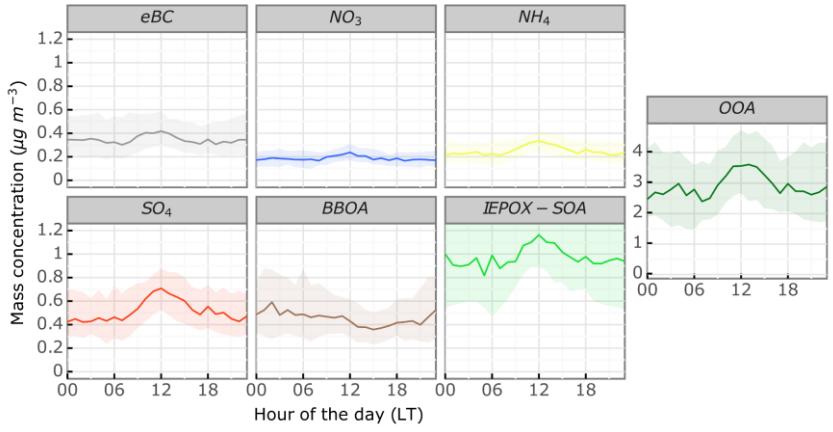

Formatted: Font color: Black

Formatted: Normal, Border: Top: (No border), Bottom: (No border), Left: (No border), Right: (No border), Between : (No border), Tab stops: 3.13", Centered + 6.27", Right

Figure 4: ~~Diurnal~~**daily profile (local time) of the PMF derived statistical factors, the inorganic chemical species and eBC mass concentrations for the whole period of measurements (1 August – 10 December, 2013). The lines represent mean values, and the shaded areas represent the standard deviations. The OOA factor, shown separately, has a different vertical scale to improve visualisation.**

3.2 Physical properties

The mean scattering coefficient at 637 nm in our study was 17±10 Mm^{-1} (Table 2), which is similar to the values reported for the same site and at the ATTO site during the dry season in previous years (Rizzo et al., 2013) and lower than observations close to biomass burning sources (32-80 Mm^{-1} (Artaxo et al., 2013; Ponczek et al., 2021)). In the dry season, fine mode particles predominate and are more efficient at scattering radiation than coarse mode dominated biogenic particles in the wet season ~~(Rizzo et al., 2013). The absorption coefficient mean value was 3±2 Mm^{-1} (Table 2, Figure 5, Section 2.2).~~(Rizzo et al., 2013). The σ_a mean value was 3±2 Mm^{-1} (Table 2, Figure 5c, Section 2.2), in accordance with low values previously reported for aged biomass burning haze (Formenti et al., 2003).

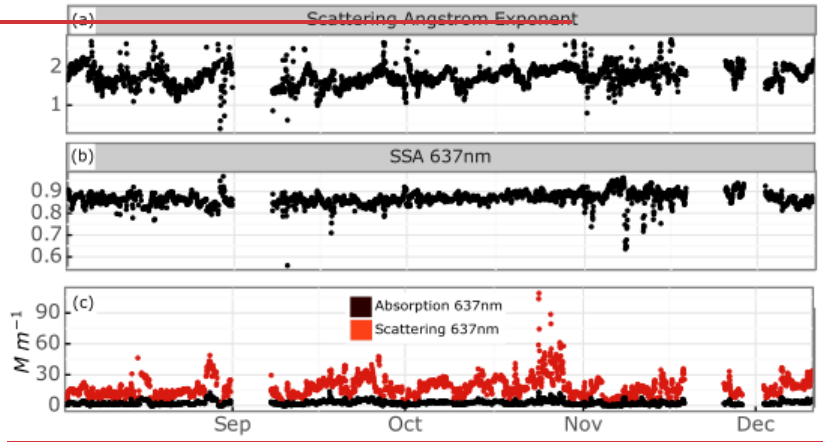

Formatted: Font: 9 pt, Bold, Font color: Black

Formatted: Font: 9 pt, Bold, Font color: Black

Formatted: Normal, Space After: 10 pt, Line spacing: single, Border: Top: (No border), Bottom: (No border), Left: (No border), Right: (No border), Between : (No border)

Formatted: Font: 9 pt, Bold, Font color: Black, English (United Kingdom)

Formatted: Font: 9 pt, Bold, Font color: Black, English (United Kingdom)

Formatted: Font: 9 pt, Bold, Font color: Black

Formatted: English (United Kingdom)

Formatted: Adjust space between Latin and Asian text, Adjust space between Asian text and numbers

Formatted: English (United Kingdom)

Formatted: Font color: Black

Formatted: Normal, Border: Top: (No border), Bottom: (No border), Left: (No border), Right: (No border), Between : (No border), Tab stops: 3.13", Centered + 6.27", Right

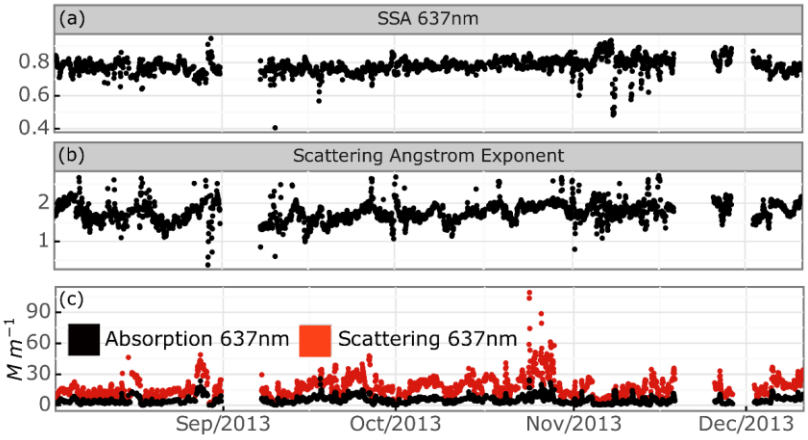

Figure 5: Time series of: a) the Scattering ~~Angstrom~~Angström Exponent (~~unitless~~SAE), b) Single Scattering Albedo (SSA) at 637 nm ~~(unitless),~~ and c) absorption and scattering coefficients at 637 nm ~~(Mm^{-1})~~.

~~The mean SSA observed in our study (0.87±0.03, Table 2) was very similar to the SSA reported for the nearby ATTO site (Saturno et al., 2018b). In previous years (2009-2012) at the same site as in our study, SSA varied from 0.84 to 0.91 from the wet to the dry season respectively. The dominance of organics and the relatively high SO_4 fraction in our study (9%, Table 1) are probably important factors for the high SSA (Artaxo et al., 2013; Rizzo et al., 2013). SSA was lower (0.77±0.08 at 637 nm) during the transition from dry to wet season in a site highly impacted by fires in southwestern Amazonia (Ponczek et al., 2021).~~

~~The mean value for the scattering Angstrom~~The mean SSA observed in our study (0.87±0.03, Table 2) was very similar to the SSA reported for a nearby site in Amazonia, as well as sites impacted by fires or urban pollution (Carrico et al., 2003; Deng et al., 2016; Kim, 2015; Kleinman et al., 2020; Nakayama et al., 2010; Saturno et al., 2018b; Wang et al., 2017; Zhu et al., 2015). The dominance of organics and the relatively high SO_4 fraction in our study (9%, Table 1) are probably important factors contributing to the high SSA (Artaxo et al., 2013; Rizzo et al., 2013), and aged biomass burning plumes have been demonstrated to be more efficient in scattering radiation than freshly emitted particles (Formenti et al., 2003). Mean SSA was lower (0.77±0.08 at 637 nm) in a site highly impacted by fires in southwestern Amazonia (Ponczek et al., 2021). In urban environments impacted by pollution, SSA was 0.92-0.89 (Tian et al., 2022), and 0.75-0.84 when the urban pollution was mixed with biomass burning (Pani et al., 2023). Slightly higher SSA values are related to urban haze episodes with high AS contributions, rural areas dominated by dust plumes, or high altitude regions influenced by clean maritime air masses (Fan et al., 2010; Han et al., 2015; Park et al., 2019). Lower SSA values were influenced by highly absorbing urban pollution (Andreae

Formatted: English (United Kingdom)

Formatted: English (United Kingdom)

Formatted: English (United Kingdom)

Formatted: Adjust space between Latin and Asian text, Adjust space between Asian text and numbers

Formatted: English (United Kingdom)

Formatted: English (United Kingdom)

Formatted: Font color: Black

Formatted: Normal, Border: Top: (No border), Bottom: (No border), Left: (No border), Right: (No border), Between : (No border), Tab stops: 3.13", Centered + 6.27", Right

et al., 2008; Cho et al., 2017; Gao et al., 2015; Jing et al., 2015; Ma et al., 2011; Ram et al., 2016; Soni et al., 2010; Titos et al., 2012) or maritime regions impacted by biomass burning from Africa (Dobracki et al., 2023).

The mean value for the scattering Angström exponent in our study was 1.76±0.26 (Table 2), which is very similar to the 1.70±0.41 and the 1.71±0.24 measured in the dry seasons of previous years at the same site and at the nearby ATTO station (Rizzo et al., 2013; Saturno et al., 2018b)(Rizzo et al., 2013; Saturno et al., 2018b), and the 1.65±0.37 measured during the dry season at a site more impacted by forest fires (Ponczek et al., 2021)(Ponczek et al., 2021). However, it was higher than the 1.48±1.12 (although within the high variability range) and the 1.29±0.50 measured in wet seasons of previous years at the same station and the ATTO site (Rizzo et al., 2013; Saturno et al., 2018b).(Rizzo et al., 2013; Saturno et al., 2018b). Higher scattering AngstromAngström exponent values are usually related to a greater proportion of fine mode particles in the aerosol population (Andreae et al., 2015), and in our case, it is probably related to the occurrence of fresh biomass burning particles.

Table 2 – Optical properties mean and standard deviation (in parentheses) for the whole studystudied period for different wavelengths.

Optical property	Wavelength (nm)	Mean
Scattering coefficient (Mm^{-1})	450	32±19
Scattering coefficient (Mm^{-1})	550	22±13
Scattering coefficient (Mm^{-1})	637	17±10
Scattering coefficient (Mm^{-1})	700	14±8
Absorption coefficient (Mm^{-1})	637	3±2
Single Scattering Albedo (Mm^{-1})	637	0.87±0.03
Scattering AngstromAngström Exponent		1.76±0.26

3.3 Chemical-dependent optical properties

We applied the multiple linear regression (Section 2.4.2) to our dataset and the resulting coefficients successfully predicted the observed scattering (Figure 6), confirming the validation of this methodology to estimate the specific contribution of each chemical group to the optical properties. All the coefficients of the multilinear regression of all the wavelengths were statistically significant ($p < 0.001$) for both MSE and MEE. The MSE of the PMF factors decreased as a function of wavelength (Figure 7), in agreement with a previous study (Ponczek et al., 2021). Regarding the inorganic species, this decrease was also observed in the AN, but absent in the AS, which showed no wavelength dependency (Figure 7). The highest MSE values were attributed to eBC (Table 3, Figure 7a), followed by the BBOA. The MSE values of the eBC, BBOA and OOA components calculated in our study at 637 nm were *circa* 180%, 67% and 43% respectively compared to (Ponczek et al., 2021). MSE of

Formatted: English (United Kingdom)
Formatted: Default Paragraph Font, Font: Times New Roman, 8 pt
Formatted: English (United Kingdom)
Formatted: English (United Kingdom)
Formatted: English (United Kingdom)
Formatted: English (United Kingdom)
Formatted: English (United Kingdom)
Formatted: English (United Kingdom)
Formatted: Font: 10 pt, English (United Kingdom)
Formatted: Adjust space between Latin and Asian text, Adjust space between Asian text and numbers
Formatted Table
Formatted: Font: 10 pt, English (United Kingdom)
Formatted: Adjust space between Latin and Asian text, Adjust space between Asian text and numbers
Formatted: Font: 10 pt, English (United Kingdom)
Formatted: Adjust space between Latin and Asian text, Adjust space between Asian text and numbers
Formatted: Font: 10 pt, English (United Kingdom)
Formatted: Adjust space between Latin and Asian text, Adjust space between Asian text and numbers
Formatted: Font: 10 pt, English (United Kingdom)
Formatted: Adjust space between Latin and Asian text, Adjust space between Asian text and numbers
Formatted: Font: 10 pt, English (United Kingdom)
Formatted: Adjust space between Latin and Asian text, Adjust space between Asian text and numbers
Formatted: Font: 10 pt, English (United Kingdom)
Formatted: Adjust space between Latin and Asian text, Adjust space between Asian text and numbers
Formatted: Font: 10 pt, English (United Kingdom)
Formatted: Font: 10 pt, English (United Kingdom)
Formatted: Adjust space between Latin and Asian text, Adjust space between Asian text and numbers
Formatted: English (United Kingdom)
Formatted: Font color: Black
Formatted: Normal, Border: Top: (No border), Bottom: (N border), Left: (No border), Right: (No border), Between : (border), Tab stops: 3.13", Centered + 6.27", Right

~~AS in our study was between 4.58-4.79 $m^2 g^{-1}$ (considering wavelengths from 450-700 nm, Table 4), which is almost double of the 2.5±0.6 $m^2 g^{-1}$ fine mode average of 93 observations of a variety of regions (urban, remote, rural continental, ocean/marine) and seasons, and using different methods, mostly at 550 nm (Hand and Malm, 2007). Despite the small variability, lower MSE was reported for drier and cleaner environments, and higher MSE was found in more polluted regions and larger particle sizes (Hand and Malm, 2007), which may partially explain the higher values found in our study – in a wet climate and during the forest fires season when the atmosphere can resemble that of highly polluted regions (Artaxo et al., 2013). A recent study in an area highly impacted by urban pollution in France reported MSE for AS ranging from 4.8-7.1 $m^2 g^{-1}$ (450-635 nm) (Velazquez-Garcia et al., 2023), resembling more similar results to our study for the lower wavelengths. Concerning the contribution of AN to the PM1 mass concentration, we tested the MLR removing AN, and the results were comparable, especially for eBC (Supplement Table S5.1). We also tested the robustness of the method by running 100 times MLR on random 50% of the data, yielding similar results (Supplement Table S5.2).~~

~~Aerosol particles which typically absorb radiation are also known to have significant scattering efficiencies, highly dependent on their sizes (Bond and Bergstrom, 2006). Biomass burning aerosols have been previously associated with high scattering efficiencies (Hand and Malm, 2007; Malm et al., 2005). However, no clear particle size dependency was observed for the radiation scattering in our study (Figure 6). Our result of a pronounced MSE of the eBC represents an opposite trend than the observed in the transition from the dry to the wet season at a site more impacted by the fires, where the MSE of BBOA was higher than eBC's (Ponczek et al., 2021).~~

~~When the mass concentration is considered, the relative contribution of eBC to the scattering in all the measured wavelengths is about 20-25% or the total scattering (Figure 7b), comparable to Southwestern Amazonia (Ponczek et al., 2021), despite our site having a significantly lower eBC concentration. The contribution of AS and AN to MSE was from 20% to 30% with increasing wavelength (Figure 7b), less than half of that in urban sites in Europe (e.g. 67% in Northern France, (Velazquez-Garcia et al., 2023), but about twice as high as during an extreme pollution haze episode in Beijing (Wang et al., 2015).~~

We applied the multiple linear regression (Section 2.4.2) to our dataset, and the resulting coefficients successfully predicted the observed scattering (R^2 = 0.86, Figure 6), confirming the validation of this methodology to estimate the specific contribution of each chemical group to the optical properties. We tested the MLR removing AN (due to its low contribution to the PM1 mass concentration, close to the ACSM detection limit, and therefore, possible artifacts), and the results were comparable, especially for eBC (Supplement Table S5.1). We also tested the robustness of the method by running 100 times MLR on randomly selected 50% of the data, yielding similar results (Supplement Table S5.2). All standard errors were small (Table 3), and the Variance Inflation Factor was around 3 for IEPOX-SOA, BBOA, AS and AN; 5.20 for OOA, and 6.19 for eBC. The abovementioned tests suggest that typical MLR caveats such as collinearity had minimal effect on the observed final results. No clear particle size dependency was observed for the radiation scattering in most of the cases (regression fitting under typical conditions, of aerosol sizes in the range of 100-150 nm), except at events dominated by ultra fine particles, at around 50 nm (Figure 6). This is notably an underestimation of observed scattering at lower particle diameters.

Formatted: Font color: Black

Formatted: Normal, Border: Top: (No border), Bottom: (N border), Left: (No border), Right: (No border), Between : (border), Tab stops: 3.13", Centered + 6.27", Right

The highest MSE values were attributed to eBC (Table 3, Figure 7a), followed by the BBOA. Previous studies on plumes dominated by either urban pollution or mixed with biomass burning presented MSE around 4.4 $m^2 g^{-1}$, dominated by organic particles (Cheng et al., 2015; Pani et al., 2023; Tao et al., 2019). The MSE values of the eBC, BBOA and OOA components calculated in our study at 637 nm were *circa* 180%, 67% and 43% respectively compared to previous measurements in Amazonia, highly impacted by biomass burning (Ponczek et al., 2021). MSE of AS in our study was between 4.58-4.79 $m^2 g^{-1}$ (Table 3, Figure 7a), in very good agreement with the MSE described for fine-mode ambient AS particles in an urban environment (Tao et al., 2019). Our result is in the lower range of the MSE described in regions impacted by urban pollution (4.8-7.1 $m^2 g^{-1}$, (Velazquez-Garcia et al., 2023), probably due to the smaller mean diameter found in our study (Figure 6). However, other regions (urban, remote, rural continental, ocean/marine) presented much smaller MSE values for AS (Cheng et al., 2015; Hand and Malm, 2007). MSE for AN at 550 nm in our study (4.79 $m^2 g^{-1}$, Table 3) is in very good agreement with the MSE found in AN in a urban pollution plume (Tao et al., 2019), and within the range previously described in regions highly impacted by urban pollution (Cheng et al., 2015; Tian et al., 2022) and a mixture of urban pollution and biomass burning (Pani et al., 2023).

The organic particles presented higher MSE for freshly emitted aerosols (BBOA) than for oxygenated particles (OOA) (Table 3), an opposite trend to what was found at PM2.5 in a region impacted by urban pollution (Tian et al., 2022). However, previous studies in Amazonia demonstrated that the size distribution of the particles is mainly below 200 nm, and even aging processes do not appear to cause an overall increase in total particles diameter, probably due to the type of the vegetation, the precursors of SOA, disintegration of larger particles, and other factors (Artaxo et al., 2013; Brito et al., 2014). Fresh biomass burning plumes at 532 nm presented a MSE range of 1.5-5.7 $m^2 g^{-1}$, depending on the fuel type, and plume age (Levin et al., 2010), and the MSE of BBOA found in our study for 550 nm is 5.33 $m^2 g^{-1}$ (Table 3). A review of MSE biomass burning plumes revealed higher MSE values for more aged plumes (Reid et al., 2005). Fine-mode organic aerosols in an urban environment presented a mean MSE of 4.6 $m^2 g^{-1}$ at wavelength 550 nm (Tao et al., 2019), closer to our BBOA MSE (Table 3).

The pronounced MSE of the eBC (7.62-13.58 $m^2 g^{-1}$, Table 3) is strongly corroborated by other studies which found remarkably high scattering efficiency related to BC, especially when the particles undergo atmospheric processing and aging, such as in the case of our study (Bond and Bergstrom, 2006; He et al., 2015; Malm et al., 2005; Pitchford et al., 2007; Romshoo et al., 2021; Schwarz et al., 2006). It has been demonstrated that while aerosol scattering efficiency increases with increasing size, age and distance from the source, the absorption efficiency remains nearly constant (Kleinman et al., 2020; Zhang et al., 2020). MSE of elemental carbon in a rural area ranged from 5.4-66.2 $m^2 g^{-1}$, and the high increase was found to be related to sulfate addition during cloud processing (Yu et al., 2010). Recently, on a comparable method, MSE for eBC has been estimated at 6 $m^2 g^{-1}$ in a site located in Western Amazonia. Located within the deforestation arc, the site is strongly impacted by fresh, sometimes local emissions, in contrast to regional or long-range transport of fires impacting Central Amazonia (Ponczek et al., 2021). In regions impacted by urban pollution MSE of eBC was 2.6 $m^2 g^{-1}$ (Tao et al., 2019), and found not to influence MSE for coarse mode particles (Titos et al., 2012).

Formatted: Font color: Black

Formatted: Normal, Border: Top: (No border), Bottom: (N border), Left: (No border), Right: (No border), Between : (border), Tab stops: 3.13", Centered + 6.27", Right

When the mass concentration is considered, the relative contribution of eBC to the scattering in all the measured wavelengths in our study is about 20-25% or the total scattering (Figure 7b), comparable to Southwestern Amazonia (Ponczek et al., 2021), despite our site having a significantly lower eBC concentration (but higher MSE for eBC). In this same Southwestern Amazonia site, the contributions of the OOA and BBOA to MSE were about twice as high than in our study. The contribution of AS and AN to MSE was from 20% to 30% with increasing wavelength (Figure 7b), less than half of that in urban sites in Europe (e.g. 67% in Northern France, (Velazquez-Garcia et al., 2023), but about twice as high as during an extreme pollution haze episode (Wang et al., 2015)). As shown in Figure 7a, the MSE of all components except AS decreases with increasing wavelength, which is consistent with the typical behavior of submicrometric aerosols. This spectral dependence can be attributed to Mie scattering theory, where smaller particles scatter shorter wavelengths more efficiently (Hand and Malm, 2007; Malm et al., 2005). Nonetheless, the variability in the MSE slopes among the different components reflects a complex interplay between aerosol mixing state, refractive index, and size distribution dynamics—particularly the diurnal evolution of each factor's contribution to the total aerosol population (Figure 4). It is particularly interesting that AS exhibits a distinct spectral behavior, typically associated with coarse-mode aerosols, denoting stark differences in its sources and atmospheric processing compared to the other components. Sulfate in Amazonia has been associated with secondary production from biogenic emissions and mixing with primary biogenic organic aerosols (PBOA) (Martin et al., 2010b; Pöhlker et al., 2012), as well as with coarse-mode particles such as dust and sea salt transported over long distances (Brito et al., 2014; Wu et al., 2019). It is remarkable that the MLR analysis captured this behavior, considering that the ACSM is limited to non-refractory species in the submicron range and is not particularly efficient at detecting the sources likely involved. This highlights the sensitivity of the MLR approach to broader aerosol population dynamics, which were captured by the optical instruments operating with a PM_{10} inlet, suggesting the influence of coarse-mode aerosol sources.

While the MSE of eBC does decrease with increasing wavelength (Figure 7a), its slope (or more precisely, its SAE) is lower than that of other aerosol components. As a result, eBC retains a relatively higher fractional contribution to total scattering at longer wavelengths compared to components with steeper MSE declines (Figure 7b). The absolute contribution to scattering is determined by both MSE and mass concentration, and although eBC mass concentrations are generally lower, its weaker wavelength dependence allows it to contribute proportionally more at longer wavelengths.

When considering the total light extinction (scattering + absorption), the relative contribution of eBC reaches about ~~30~~31% (Figure 8), which is comparable to the work in highly urbanized region ~~in Europe~~ (Velazquez-Garcia et al., 2023)~~, however significantly lower than the 76±20% observed in urban pollution in China (Yu et al., 2010).~~ , and an episodic biomass burning event in a rural area (Yu et al., 2010). However, it is less than half of the MEE relative contribution of BC observed during urban pollution episodes (Tian et al., 2022; Yu et al., 2010). The comparison with urban pollution particles contribution to MEE reveals that the contribution of highly oxygenated particles is very similar (*circa* 20%, Figure 8, (Tian et al., 2022)), and the most evident difference is the nitrate-based particles, with a much larger contribution in the urban pollution region (Figure 8, (Tian et al., 2022)). MEE has been shown to increase by a factor of 3 while freshly emitted smoke from fires ages in the atmosphere, reaching up to $7 m^2 g^{-1}$ at 532 wavelength (Saide et al., 2022). The OOA factor presented a relatively high

Formatted: English (United Kingdom)

Formatted: English (United Kingdom)

Formatted: English (United Kingdom)

Formatted: Font color: Black

Formatted: Normal, Border: Top: (No border), Bottom: (N border), Left: (No border), Right: (No border), Between : (border), Tab stops: 3.13", Centered + 6.27", Right

contribution to MSE and MEE (Figures 8b and 9) due to its high fraction of the total PM1 mass (Table 1), although its MSE is relatively low (Figure 7a). The contribution of AS to MSE increases with increasing wavelength (from 10% to 20%, Figure 7b), while OOA decreased (from 30% to 20%, Figure 7b).

By using the MSE and MEE ratios, we calculated specific SSA for the eBC, obtaining a value of 0.57. This means that 57% of the light extinction provoked by the eBC is scattered rather than absorbed, which is higher than the eBC specific SSA of 0.46 based on previous studies in more polluted conditions (Ponczek et al., 2021; Velazquez-Garcia et al., 2023). SSA of eBC has been described as typically ranging from 0.3 to 0.4, with higher values associated ~~to~~with heavy coating (Luo et al., 2020)~~.~~ ~~Evidence of coating increasing elemental carbon scattering efficiency has been found in the past (He et al., 2015; Yu et al., 2010), however other studies found that thick coating in eBC lowered scattering coefficients (Darbyshire et al., 2019),~~ and below 0.3 for pure black carbon (Wang et al., 2021).

~~A previous study found that eBC absorption cross-section for the Amazon was 12.3 $m^2 g^{-1}$ (Saturno et al., 2018b), and we tested our dataset applying this value. The result is that eBC mass concentrations would become half of what they are reported, with no change in σ_a, SSA, but MSE would double, while eBC contribution to MEE (Figure 8) would remain unchanged. Due to some methodology differences between our study and (Saturno et al., 2018a) (they measured refractory Black Carbon using a single-particle soot photometer SP2, with a higher cut-off, possibly leading to a sub-estimation of the mass), and the fact that applying the absorption cross-section value they found would make MSE of eBC be an order of magnitude higher than the others (Supplement Figure S6), we opted to remain with the more stablished value of 6.6 $m^2 g^{-1}$.~~

~~The OOA factor presented a relatively high relative contribution to MSE and MEE (Figures 8b and 9) due to its high mass relative contribution to the total PM1 mass (Table 1), although its MSE is relatively low (Figure 7a). Our results show an increase in AS relative fraction of contribution to MSE with increasing wavelength (from 10% to 20%, Figure 7b), while OOA decreased (from 30% to 20%, Figure 7b). The relative contributions to MSE of the OOA and BBOA were about twice as high in a site more directly impacted by fires during the dry season than in our study (Ponczek et al., 2021).~~

~~**Table 3 – MEE, MAE and MSE for different wavelengths and aerosol components with standard errors. All the coefficients were statistically significant for all the wavelengths for MSE and MEE ($p < 0.001$).**~~

A previous study found an eBC absorption cross-section in Amazonia of 12.3 $m^2 g^{-1}$ (Saturno et al., 2018b), and we tested our dataset applying this value (Supplement, Figure S6.1). The result is that eBC mass concentrations would decrease by half, with no change in σ_a and SSA, but MSE would double, while eBC contribution to MEE (Figure 8, Figure S6.2) would remain unchanged. Due to some methodology differences between our study and (Saturno et al., 2018b) (they measured refractory Black Carbon using a single-particle soot photometer SP2, with a higher cut-off, possibly leading to a sub-estimation of the mass), and the fact that applying the absorption cross-section value they found would make MSE of eBC be an order of magnitude higher than the others (Supplement Figure S6.1), we opted to remain with the more established value of 6.6 $m^2 g^{-1}$.

Formatted: English (United Kingdom)

Formatted: English (United Kingdom)

Formatted: English (United Kingdom)

Formatted: English (United Kingdom)

Formatted: Font color: Black

Formatted: Normal, Border: Top: (No border), Bottom: (N border), Left: (No border), Right: (No border), Between : (border), Tab stops: 3.13", Centered + 6.27", Right

Table 3 – MSE for different wavelengths and aerosol components with standard errors. The Variance Inflation Factor was around 3 for IEPOX-SOA, BBOA, AS and AN; 5.20 for OOA, and 6.19 for eBC, suggesting that typical MLR caveats such as collinearity had minimal effect on the observed final results.

	MSE (m^2 g^{-1})			MAE	MEE		
Wavelength (nm)	450	550	637		700	637	637
eBC	13.58±1.08	10.67±0.70	8.68±0.52		7.62±0.44	6.6	15.28±0.52
BBOA	7.96±0.33	5.33±0.21	3.83±0.16		3.10±0.13		
IEPOX-SOA	5.61±0.41	3.84±0.27	2.87±0.20		2.37±0.17		
OOA	3.58±0.15	1.94±0.10	1.24±0.07		0.90±0.06		
AS	4.79±0.62	4.79±0.41	4.77±0.30		4.58±0.25		
AN	7.07±1.41	5.17±0.92	4.41±0.68		3.93±0.58		

Deleted Cells
Deleted Cells
Formatted: Font: Times New Roman, 10 pt, English (United Kingdom)
Formatted Table
Deleted Cells
Deleted Cells
Formatted: Font: Times New Roman, 10 pt, English (United Kingdom)
Formatted: Font: Times New Roman, 10 pt, English (United Kingdom)
Formatted: Font: Times New Roman, 10 pt, English (United Kingdom)
Formatted: Font: Times New Roman, 10 pt, English (United Kingdom)
Formatted: Font: Times New Roman, 10 pt, English (United Kingdom)
Formatted: Font: Times New Roman, 10 pt, English (United Kingdom)
Formatted: Font: Times New Roman, 10 pt
Formatted: Font: Times New Roman, 10 pt, English (United Kingdom)
Formatted: English (United Kingdom)
Formatted: Tab stops: 3.11", Left

Formatted: Font color: Black
Formatted: Normal, Border: Top: (No border), Bottom: (No border), Left: (No border), Right: (No border), Between : (No border), Tab stops: 3.13", Centered + 6.27", Right

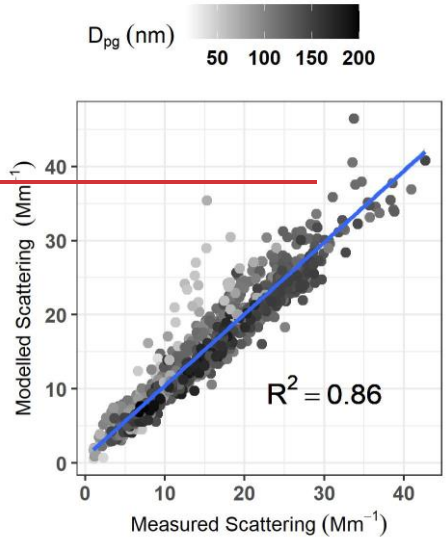

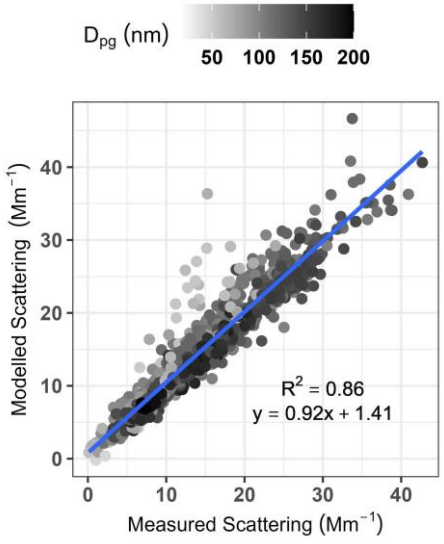

Formatted: Font color: Black

Formatted: Normal, Border: Top: (No border), Bottom: (N border), Left: (No border), Right: (No border), Between : (border), Tab stops: 3.13", Centered + 6.27", Right

Figure 6: Measured ~~radiation~~vs modelled aerosol light scattering at 637 nm ~~vs modeled scattering (MSE).~~ The gray scale corresponds to the equivalent mobility particle diameter for singly charged particles (D_{pg} section 2.2). The blue line ~~indicates a~~shows the linear ~~correlation.~~regression (slope =0.92).

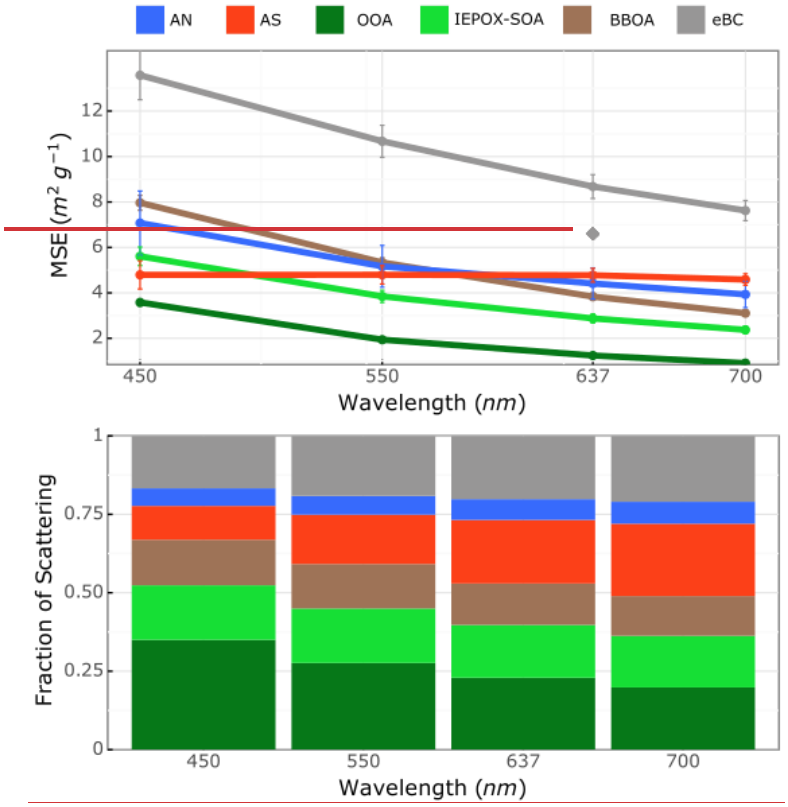

Formatted: English (United Kingdom)
Formatted: English (United Kingdom)
Formatted: English (United Kingdom)
Formatted: Adjust space between Latin and Asian text, Adjust space between Asian text and numbers
Formatted: English (United Kingdom)
Formatted: English (United Kingdom)
Formatted: Font color: Black
Formatted: Normal, Border: Top: (No border), Bottom: (No border), Left: (No border), Right: (No border), Between : (No border), Tab stops: 3.13", Centered + 6.27", Right

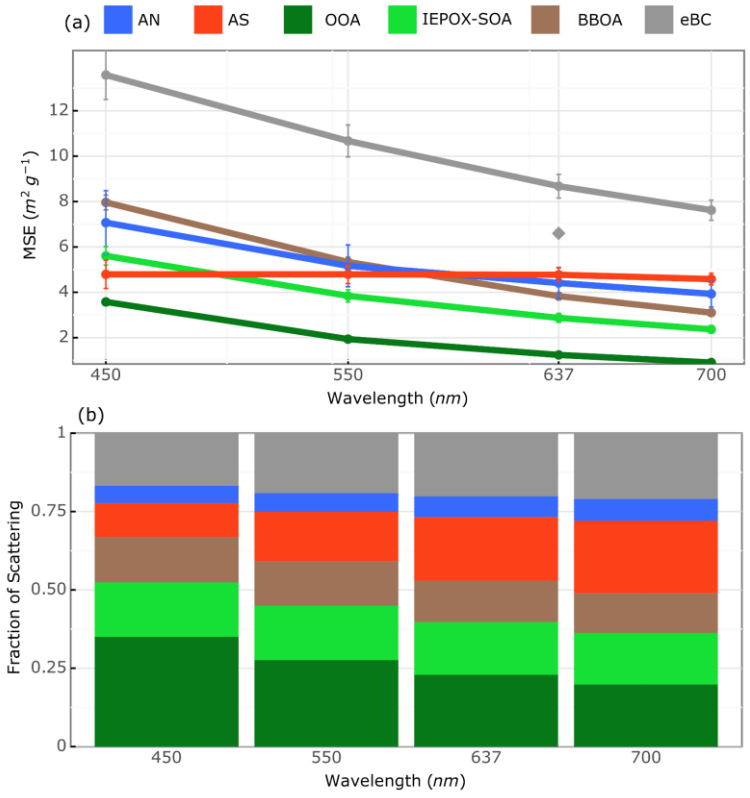

Figure 7: a) Mass scattering efficiencies ~~(MSE) for each~~of individual chemical ~~component (color~~components (colored lines) at each wavelength, where the dots are the coefficients ~~of~~obtained from the multi-linear regression, ~~the~~with bars ~~are~~indicating the standard errors, and the diamond shape ~~is~~denotes the value of absorption efficiency of ~~the~~ eBC at 637 nm; and b) the ~~fraction~~ fractional contribution of each component to total light scattering ~~of each component at each wavelength, considering its mass fraction to the total mass of submicrometer particles~~.

Formatted: English (United Kingdom)
Formatted: English (United Kingdom)
Formatted: English (United Kingdom)
Formatted: Adjust space between Latin and Asian text, Adjust space between Asian text and numbers
Formatted: English (United Kingdom)
Formatted: English (United Kingdom)
Formatted: English (United Kingdom)
Formatted: English (United Kingdom)
Formatted: English (United Kingdom)
Formatted: English (United Kingdom)
Formatted: English (United Kingdom)
Formatted: English (United Kingdom)
Formatted: Font color: Black
Formatted: Normal, Border: Top: (No border), Bottom: (N border), Left: (No border), Right: (No border), Between : (border), Tab stops: 3.13", Centered + 6.27", Right

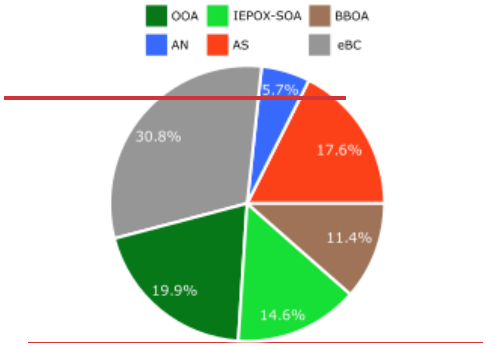

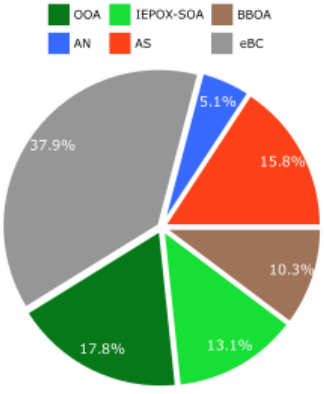

Figure 8: The relative contribution (%) of ~~extinction coefficient (scattering + absorption)~~MEE of each component considering its mass fraction to the total mass of submicrometer particles~~.~~ (Table 1).

4 Conclusions

The results have shown that the submicrometer particle mass concentration during the dry season (6.3±3.3 μg m^{-3}), which is about an order of magnitude higher than typically observed at this site during the wet season, is highly dominated by the organic fraction (77±5%). The organic aerosols were separated into 3 PMF statistical factors, identified as BBOA, OOA, and IEPOX-SOA. The OOA, associated with highly processed and oxidized particles is the dominant factor (51±6% of the PM_1),

Formatted: English (United Kingdom)
Formatted: English (United Kingdom)
Formatted: Adjust space between Latin and Asian text, Adjust space between Asian text and numbers
Formatted: English (United Kingdom)
Formatted: Font color: Black
Formatted: Normal, Border: Top: (No border), Bottom: (No border), Left: (No border), Right: (No border), Between : (No border), Tab stops: 3.13", Centered + 6.27", Right

followed by IEPOX-SOA (isoprene SOA following a low-NO route, 17±5%), while the factor more directly associated with fresh biomass burning emissions (BBOA) represents 9±5% of PM1.

The mean radiation scattering coefficient at 637 nm was 17±10 Mm^{-1}, and the mean absorption coefficient was 3±2 Mm^{-1}, which ~~are~~ is higher than what was observed in the wet season, but lower than ~~the respective coefficients measured~~ at sites much more impacted by the proximity to fresh forest fires ~~but exceed those observed during the wet season~~. The SSA of 0.87±0.03 was elevated compared to values previously described in the wet season, but generally in good agreement with SSA values of previous dry seasons~~.~~ - likely an indication of the scattering efficiency of eBC following atmospheric processing and coating. The mean scattering ~~Angstrom~~Angström exponent was 1.76±0.26, surpassing the values previously measured during the wet season, likely due to the greater relative proportion of smaller particles in the aerosol population measured in our study, compared to the primary biogenic aerosols, Saharan dust and sea salt typical of the wet season in central Amazonia.

An MLR analysis of optical properties and different species/factors yielded the highest MSE for eBC in all wavelengths (7.62-13.58 $m^2 g^{-1}$), followed by the BBOA and AN in the shorter wavelengths (450 and 550 nm), ~~with the addition of~~and by AS in the longer wavelengths (637 and 700 nm). Despite having a small mass contribution (6%), eBC dominated the MEE relative contribution (~~30.8~~37.9%), followed by the OOA (~~19.9~~17.8%). The high MSE of eBC (and a calculated specific SSA of 0.57) is ~~surprising~~remarkable, and more studies concerning the chemical processing of those particles after their emission are needed in order to understand the processes behind the outstanding efficiency of light scattering of this highly absorbing particle. A special focus should be given to the role of aerosol coating in this process.

~~While previous studies show a significant contribution of organic particles to light~~Aerosol observations at the heart of Amazonia are extremely challenging. Although our analysis during the dry season yielded robust results, limitations remain—particularly concerning the size distribution of BC and its absorption ~~(brown carbon) our study shows that the eBC can also have a significant contribution to light~~ across multiple wavelengths. To advance our understanding, future studies should prioritize extensive field and laboratory observations aimed at better constraining aerosol coating formation mechanisms and their impact on the radiative scattering~~. The~~ properties of BC particles in Amazonia. Increasing the precision of the quantification of the eBC contribution to light scattering has the potential to improve models and decrease uncertainties in global radiative forcing estimations.

~~**Code availability**~~

Codes and Data availability

~~Data will be made~~Codes and data are currently available ~~upon acceptance of the article.~~in this link: https://zenodo.org/records/15345166; DOI: 10.5281/zenodo.15345166

Formatted: English (United Kingdom)
Formatted: English (United Kingdom)
Formatted: English (United Kingdom)
Formatted: English (United Kingdom)
Formatted: English (United Kingdom)
Formatted: English (United Kingdom)
Formatted: English (United Kingdom)
Formatted: English (United Kingdom)
Formatted: English (United Kingdom)
Formatted: English (United Kingdom)
Formatted: English (United Kingdom)
Formatted: English (United Kingdom)
Formatted: English (United Kingdom)
Formatted: English (United Kingdom)
Formatted: English (United Kingdom)
Formatted: Font color: Black
Formatted: Normal, Border: Top: (No border), Bottom: (N border), Left: (No border), Right: (No border), Between : (border), Tab stops: 3.13", Centered + 6.27", Right

Author Contribution

RS, JFB, and PA conceptualized and designed the methodology. RS performed the field measurements, with the support of JFB. RS, JFB, SC, LVR and JDM applied the methodology. RS ~~wrothe~~wrote the original draft, and all the authors discussed the results and commented on the paper.

Competing Interests

Some authors are members of the editorial board of ACP.

Acknowledgments

We thank the Large-scale Biosphere-Atmosphere (LBA) project group and the Clima e Ambiente (CLIAMB) department at Instituto Nacional de Pesquisas da Amazônia (INPA) for continuous support. The Brazil-UK Network for Investigation of Amazonian Atmospheric Composition and Impacts on Climate (BUNIAACIC) project was funded by the UK Natural Environment Research Council (NERC; grant NE/I030178/1) and FAPESP (2012/14437-9, 2013/05014-0). J. Brito was funded by Fundação de Amparo à Pesquisa do Estado de São Paulo (FAPESP; project 2013/25058-1), by the Labex CaPPA project, which is funded by the French National Research Agency (ANR) through the PIA (Programme d'Investissement d'Avenir) under contract ANR-11-LABX-0005-01; the CLIMIBIO and ECRIN projects, all financed by the Regional Council "Hauts-de-France" and the European Regional Development Fund (ERDF), and the COST COLOSSAL Action (CA16109). L. Rizzo acknowledges the support of the Brazilian National Council for Reasearch (CNPq, 304819/2022-0). We thank A. Ribeiro, F. Morais, F. Jorge and S. Morais for technical and logistics support.

References

Alfarra, M. R., Coe, H., Allan, J. D., Bower, K. N., Boudries, H., Canagaratna, M. R., Jimenez, J. L., Jayne, J. T., Garforth, A. a., Li, S.-M. and Worsnop, D. R.: Characterization of urban and rural organic particulate in the Lower Fraser Valley using two Aerodyne Aerosol Mass Spectrometers, Atmos. Environ., 38(34), 5745–5758, doi:10.1016/j.atmosenv.2004.01.054, 2004.

Alfarra, M. R., Prevot, A. S. H., Szidat, S., Sandradewi, J., Weimer, S., Lanz, V. a., Schreiber, D., Mohr, M. and Baltensperger, U.: Identification of the Mass Spectral Signature of Organic Aerosols from Wood Burning Emissions, Environ. Sci. Technol., 41(16), 5770–5777, doi:10.1021/es062289b, 2007.

Allan, J. D., Bower, K. N., Coe, H., Boudries, H., Jayne, J. T., Canagaratna, M. R., Millet, D. B., Goldstein, A. H., Quinn, P. K., Weber, R. J. and Worsnop, D. R.: Submicron aerosol composition at Trinidad Head, California, during ITCT 2K2: Its relationship with gas phase volatile organic carbon and assessment of instrument performance, J. Geophys. Res. Atmos., 109(D23), n/a--n/a, doi:10.1029/2003JD004208, 2004.

Formatted: English (United Kingdom)

Formatted: English (United Kingdom)

Formatted: Font color: Black, Kern at 16 pt

Formatted: Font color: Black, English (United Kingdom), Kern at 16 pt

Formatted: English (United Kingdom)

Formatted: Font: 9 pt, Bold, Font color: Black, English (United States)

Formatted: Font color: Black

Formatted: Normal, Border: Top: (No border), Bottom: (No border), Left: (No border), Right: (No border), Between : (No border), Tab stops: 3.13", Centered + 6.27", Right

Allan, J. D., Morgan, W. T., Darbyshire, E., Flynn, M. J., Williams, P. I., Oram, D. E., Artaxo, P., Brito, J., Lee, J. D. and Coe, H.: Airborne observations of IEPOX-derived isoprene SOA in the Amazon during SAMBBA, Atmos. Chem. Phys., 14(20), 11393–11407, doi:10.5194/acp-14-11393-2014, 2014.

Anderson, T. L. and Ogren, J. A.: Determining Aerosol Radiative Properties Using the TSI 3563 Integrating Nephelometer, Aerosol Sci. Technol., 29(1), 57–69, doi:10.1080/02786829808965551, 1998.

Andreae, M. O.: The Biosphere: Pilot or passenger on spaceship Earth?, Contrib. to Glob. Chang. Res., (January 2001), 59–66, 2001.

Andreae, M. O., Schmid, O., Yang, H., Chand, D., Zhen Yu, J., Zeng, L. M. and Zhang, Y. H.: Optical properties and chemical composition of the atmospheric aerosol in urban Guangzhou, China, Atmos. Environ., 42(25), 6335–6350, doi:10.1016/j.atmosenv.2008.01.030, 2008.

Andreae, M. O., Acevedo, O. C., Araùjo, A., Artaxo, P., Barbosa, C. G. G., Barbosa, H. M. J., Brito, J., Carbone, S., Chi, X., Cintra, B. B. L., da Silva, N. F., Dias, N. L., Dias-Júnior, C. Q., Ditas, F., Ditz, R., Godoi, a. F. L., Godoi, R. H. M., Heimann, M., Hoffmann, T., Kesselmeier, J., Könemann, T., Krüger, M. L., Lavric, J. V, Manzi, a. O., Lopes, a. P., Martins, D. L., Mikhailov, E. F., Moran-Zuloaga, D., Nelson, B. W., Nölscher, a. C., Santos Nogueira, D., Piedade, M. T. F., Pöhlker, C., Pöschl, U., Quesada, C. a., Rizzo, L. V, Ro, C.-U., Ruckteschler, N., Sá, L. D. a., de Oliveira Sá, M., Sales, C. B., dos Santos, R. M. N., Saturno, J., Schöngart, J., Sörgel, M., de Souza, C. M., de Souza, R. a. F., Su, H., Targhetta, N., Tóta, J., Trebs, I., Trumbore, S., van Eijck, A., Walter, D., Wang, Z., Weber, B., Williams, J., Winderlich, J., Wittmann, F., Wolff, S. and Yáñez-Serrano, a. M.: The Amazon Tall Tower Observatory (ATTO): overview of pilot measurements on ecosystem ecology, meteorology, trace gases, and aerosols, Atmos. Chem. Phys., 15(18), 10723–10776, doi:10.5194/acp-15-10723-2015, 2015.

~~Aragão, L. E. O. C., Anderson, L. O., Lima, A. and Arai, E.: Fires in Amazonia, pp. 301–329., 2016.~~

Araújo, A. C., Nobre, A. D., Krujit, B., Elbers, A., Dallarosa, R., Stefani, P., von Randow, C., Manzi, A. O., Culf, A. D., Gash, J. H. C., Valentini, R. and Kabat, P.: Comparative measurements of carbon dioxide fluxes from two nearby towers in a central Amazonian rainforest: The Manaus LBA site, J. Geophys. Res., 107(D20), doi:10.1029/2001JD000676, 2002.

Artaxo, P., Rizzo, L. V., Brito, J. F., Barbosa, H. M. J., Arana, A., Sena, E. T., Cirino, G. G., Bastos, W., Martin, S. T. and Andreae, M. O.: Atmospheric aerosols in Amazonia and land use change: from natural biogenic to biomass burning conditions, Faraday Discuss., 165, 203, doi:10.1039/c3fd00052d, 2013.

~~Berenguer, E., Armenteras, D., Lees, A. C., Smith, C. C., Fearnside, P., Nascimento, N., Alencar, A., Almeida, C., Aragão, L. E. O., Barlow, J., Bilbao, B., Brando, P. M., Bynoe, P., Finer, M., Flores, B. M., Jenkins, C. N., Silva Junior, C. H. L., Souza, C. and García-Villacorta, R.: Chapter 19: Drivers and ecological impacts of deforestation and forest degradation., 2021.~~

Bond, T. C. and Bergstrom, R. W.: Light absorption by carbonaceous particles: An investigative review, Aerosol Sci. Technol., 40(1), 27–67, doi:10.1080/02786820500421521, 2006.

Brito, J., Rizzo, L. V., Morgan, W. T., Coe, H., Johnson, B., Haywood, J., Longo, K., Freitas, S., Andreae, M. O. and Artaxo, P.: Ground-based aerosol characterization during the South American Biomass Burning Analysis (SAMBBA) field experiment, Atmos. Chem. Phys., 14(22), 12069–12083, doi:10.5194/acp-14-12069-2014, 2014.

Brito, J., Freney, E., Dominutti, P., Borbon, A., Haslett, S. L., Batenburg, A. M., Colomb, A., Dupuy, R., Denjean, C., Burnet, F., Bourriane, T., Deroubaix, A., Sellegri, K., Borrmann, S., Coe, H., Flamant, C., Knippertz, P. and Schwarzenboeck, A.: Assessing the role of anthropogenic and biogenic sources on PM 1 over southern West Africa using aircraft measurements, Atmos. Chem. Phys, 18, 757–772, doi:10.5194/acp-18-757-2018, 2018.

Budisulistiorini, S. H., Canagaratna, M. R., Croteau, P. L., Marth, W. J., Baumann, K., Edgerton, E. S., Shaw, S. L., Knipping, E. M., Worsnop, D. R., Jayne, J. T., Gold, A. and Surratt, J. D.: Real-time continuous characterization of secondary organic aerosol derived from isoprene epoxydiols in downtown Atlanta, Georgia, using the aerodyne aerosol chemical speciation monitor, Environ. Sci. Technol., 47(11), 5686–5694, doi:10.1021/es400023n, 2013.

Caravan, R. L., Bannan, T. J., Winiberg, F. A. F., Khan, M. A. H., Rousso, A. C., Jasper, A. W., Worrall, S. D., Bacak, A., Artaxo, P., Brito, J., Priestley, M., Allan, J. D., Coe, H., Ju, Y., Osborn, D. L., Hansen, N., Klippenstein, S. J., Shallcross, D. E., Taatjes, C. A. and Percival, C. J.: Observational evidence for Criegee intermediate oligomerization reactions relevant to aerosol formation in the troposphere, Nat.

Formatted: Font color: Black

Formatted: Normal, Border: Top: (No border), Bottom: (N border), Left: (No border), Right: (No border), Between : (border), Tab stops: 3.13", Centered + 6.27", Right

Geosci., 1, doi:10.1038/s41561-023-01361-6, 2024.

Carbone, S., Saarikoski, S., Frey, A., Reyes, F., Reyes, P., Castillo, M., Gramsch, E., Oyola, P., Jayne, J., Worsnop, D. R. and Hillamo, R.: Chemical Characterization of Submicron Aerosol Particles in Santiago de Chile, Aerosol Air Qual. Res., 462–473, doi:10.4209/aaqr.2012.10.0261, 2013.

Carrico, C. M., Bergin, M. H., Xu, J., Baumann, K. and Maring, H.: Urban aerosol radiative properties: Measurements during the 1999 Atlanta supersite experiment, J. Geophys. Res. Atmos., 108(7), 1–17, doi:10.1029/2001jd001222, 2003.

Chen, G., Canonaco, F., Tobler, A., Aas, W., Alastuey, A., Allan, J., Atabakhsh, S., Aurela, M., Baltensperger, U., Bougiatioti, A., De Brito, J. F., Ceburnis, D., Chazeau, B., Chebaicheb, H., Daellenbach, K. R., Ehn, M., El Haddad, I., Eleftheriadis, K., Favez, O., Flentje, H., Font, A., Fossum, K., Freney, E., Gini, M., Green, D. C., Heikkinen, L., Herrmann, H., Kalogridis, A.-C., Keernik, H., Lhotka, R., Lin, C., Lunder, C., Maasikmets, M., Manousakas, M. I., Marchand, N., Marin, C., Marmureanu, L., Mihalopoulos, N., Močnik, G., Nęcki, J., O'Dowd, C., Ovadnevaite, J., Peter, T., Petit, J.-E., Pikridas, M., Matthew Platt, S., Pokorná, P., Poulain, L., Priestman, M., Riffault, V., Rinaldi, M., Różański, K., Schwarz, J., Sciare, J., Simon, L., Skiba, A., Slowik, J. G., Sosedova, Y., Stavroulas, I., Styszko, K., Teinemaa, E., Timonen, H., Tremper, A., Vasilescu, J., Via, M., Vodička, P., Wiedensohler, A., Zografou, O., Cruz Minguillón, M. and Prévôt, A. S. H.: European aerosol phenomenology − 8: Harmonised source apportionment of organic aerosol using 22 Year-long ACSM/AMS datasets, Environ. Int., 166(May), 107325, doi:10.1016/j.envint.2022.107325, 2022.

Chen, Q., Farmer, D. K., Schneider, J., Zorn, S. R., Heald, C. L., Karl, T. G., Guenther, a., Allan, J. D., Robinson, N., Coe, H., Kimmel, J. R., Pauliquevis, T., Borrmann, S., Pöschl, U., Andreae, M. O., Artaxo, P., Jimenez, J. L. and Martin, S. T.: Mass spectral characterization of submicron biogenic organic particles in the Amazon Basin, Geophys. Res. Lett., 36(20), L20806, doi:10.1029/2009GL039880, 2009.

Chen, Q., Farmer, D. K., Rizzo, L. V., Pauliquevis, T., Kuwata, M., Karl, T. G., Guenther, a., Allan, J. D., Coe, H., Andreae, M. O., Pöschl, U., Jimenez, J. L., Artaxo, P. and Martin, S. T.: Submicron particle mass concentrations and sources in the Amazonian wet season (AMAZE-08), Atmos. Chem. Phys., 15(7), 3687–3701, doi:10.5194/acp-15-3687-2015, 2015.

Cheng, Y. F., Wiedensohler, A., Eichler, H., Su, H., Gnauk, T., Brüggemann, E., Herrmann, H., Heintzenberg, J., Slanina, J., Tuch, T., Hu, M. and Zhang, Y. H.: Aerosol optical properties and related chemical apportionment at Xinken in Pearl River Delta of China, Atmos. Environ., 42(25), 6351–6372, doi:10.1016/j.atmosenv.2008.02.034, 2008.

Cheng, Z., Jiang, J., Chen, C., Gao, J., Wang, S., Watson, J. G., Wang, H., Deng, J., Wang, B., Zhou, M., Chow, J. C., Pitchford, M. L. and Hao, J.: Estimation of aerosol mass scattering efficiencies under high mass loading: Case study for the megacity of Shanghai, China, Environ. Sci. Technol., 49(2), 831–838, doi:10.1021/es504567q, 2015.

Cho, C., Kim, S. W., Rupakheti, M., Park, J. S., Panday, A., Yoon, S. C., Kim, J. H., Kim, H., Jeon, H., Sung, M., Mann Kim, B., Hong, S. K., Park, R. J., Rupakheti, D., Singh Mahata, K., Siva Praveen, P., Lawrence, M. G. and Holben, B.: Wintertime aerosol optical and radiative properties in the Kathmandu Valley during the SusKat-ABC field campaign, Atmos. Chem. Phys., 17(20), 12617–12632, doi:10.5194/acp-17-12617-2017, 2017.

Cubison, M. J., Ortega, a. M., Hayes, P. L., Farmer, D. K., Day, D., Lechner, M. J., Brune, W. H., Apel, E., Diskin, G. S., Fisher, J. a., Fuelberg, H. E., Hecobian, a., Knapp, D. J., Mikoviny, T., Riemer, D., Sachse, G. W., Sessions, W., Weber, R. J., Weinheimer, a. J., Wisthaler, a. and Jimenez, J. L.: Effects of aging on organic aerosol from open biomass burning smoke in aircraft and laboratory studies, Atmos. Chem. Phys., 11(23), 12049–12064, doi:10.5194/acp-11-12049-2011, 2011.

Darbyshire, E., Morgan, W. T., Allan, J. D., Liu, D., Flynn, M. J., Dorsey, J. R., O'Shea, S. J., Lowe, D., Szpek, K., Marenco, F., Johnson, B. T., Bauguitte, S., Haywood, J. M., Brito, J. F., Artaxo, P., Longo, K. M. and Coe, H.: The vertical distribution of biomass burning pollution over tropical South America from aircraft in situ measurements during SAMBBA, Atmos. Chem. Phys., 19(9), 5771–5790, doi:10.5194/acp-19-5771-2019, 2019.

~~Davidson, E. a, de Araújo, A. C., Artaxo, P., Balch, J. K., Brown, I. F., C Bustamante, M. M., Coe, M. T., DeFries, R. S., Keller, M., Longo, M., Munger, J. W., Schroeder, W., Soares-Filho, B. S., Souza, C. M. and Wofsy, S. C.: The Amazon basin in transition., Nature, 481(7381), 321–8, doi:10.1038/nature10717, 2012.~~

Deng, J., Zhang, Y., Hong, Y., Xu, L., Chen, Y., Du, W. and Chen, J.: Optical properties of PM2.5 and the impacts of chemical compositions in the coastal city Xiamen in China, Sci. Total Environ., 557–558, 665–675, doi:10.1016/j.scitotenv.2016.03.143, 2016.

Formatted: Font color: Black

Formatted: Normal, Border: Top: (No border), Bottom: (N border), Left: (No border), Right: (No border), Between : (border), Tab stops: 3.13", Centered + 6.27", Right

Denjean, C., Brito, J., Libois, Q., Mallet, M., Bourrianne, T., Burnet, F., Dupuy, R., Flamant, C. and Knippertz, P.: Unexpected Biomass Burning Aerosol Absorption Enhancement Explained by Black Carbon Mixing State, Geophys. Res. Lett., 47(19), 1–11, doi:10.1029/2020GL089055, 2020.

Dobracki, A., Zuidema, P., Howell, S. G., Saide, P., Freitag, S., Aiken, A. C., Burton, S. P., Sedlacek, A. J., Redemann, J. and Wood, R.: An attribution of the low single-scattering albedo of biomass burning aerosol over the southeastern Atlantic, Atmos. Chem. Phys., 23(8), 4775–4799, doi:10.5194/acp-23-4775-2023, 2023.

Draxler, R. R. and Hess, G. D.: An overview of the HYSPLIT_4 modelling system for trajectories, dispersion and deposition, Aust. Meteorol. Mag., 47(4), 295–308, 1998.

F. G. Assis, L. F., Ferreira, K. R., Vinhas, L., Maurano, L., Almeida, C., Carvalho, A., Rodrigues, J., Maciel, A. and Camargo, C.: TerraBrasilis: A Spatial Data Analytics Infrastructure for Large-Scale Thematic Mapping, ISPRS Int. J. Geo-Information, 8(11), 513, doi:10.3390/ijgi8110513, 2019.

Fan, X., Chen, H., Xia, X., Li, Z. and Cribb, M.: Aerosol optical properties from the Atmospheric Radiation Measurement Mobile Facility at Shouxian, China, J. Geophys. Res. Atmos., 115(24), doi:10.1029/2010JD014650, 2010.

Fisch, G., Tota, J., Machado, L. a. T., Silva Dias, M. a. F., da F. Lyra, R. F., Nobre, C. a., Dolman, a. J. and Gash, J. H. C.: The convective boundary layer over pasture and forest in Amazonia, Theor. Appl. Climatol., 78(1–3), 47–59, doi:10.1007/s00704-004-0043-x, 2004.

Flores, B. M., Montoya, E., Sakschewski, B., Nascimento, N., Staal, A., Betts, R. A., Levis, C., Lapola, D. M., Esquível-Muelbert, A., Jakovac, C., Nobre, C. A., Oliveira, R. S., Borma, L. S., Nian, D., Boers, N., Hecht, S. B., ter Steege, H., Arieira, J., Lucas, I. L., Berenguer, E., Marengo, J. A., Gatti, L. V., Mattos, C. R. C. and Hirota, M.: Critical transitions in the Amazon forest system, Nature, 626(7999), 555–564, doi:10.1038/s41586-023-06970-0, 2024.

Formenti, P., Elbert, W., Maenhaut, W., Haywood, J., Osborne, S. and Andreae, M. O.: Inorganic and carbonaceous aerosols during the Southern African Regional Science Initiative (SAFARI 2000) experiment: Chemical characteristics, physical properties, and emission data or smoke from African biomass burning, J. Geophys. Res. D Atmos., 108(13), doi:10.1029/2002jd002408, 2003.

Forster, P. M., Storelvmo, T., Armour, K., Collins, W., Dufresne, J.-L., Frame, D., Lunt, D. J., Mauritsen, T., Palmer, M. D., Watanabe, M., Wild, M. and Zhang, H.: The Earth's Energy Budget, Climate Feedbacks and Climate Sensitivity, in Climate Change 2021 – The Physical Science Basis. Contribution of Working Group I to the Sixth Assessment Report of the Intergovernmental Panel on Climate Change [Masson-Delmotte, V., P. Zhai, A. Pirani, S.L. Connors, C. Pean, S. Berger, N. Caud, Y. Chen, pp. 923–1054, Cambridge University Press, Cambridge and New York., 2021.

Fuzzi, S., Decesari, S., Facchini, M. C., Cavalli, F., Emblico, L., Mircea, M., Andreae, M. O., Trebs, I., Hoffer, A., Guyon, P., Artaxo, P., Rizzo, L. V~~,~~ Lara, L. L., Pauliquevis, T., Maenhaut, W., Raes, N., Chi, X., Mayol-Bracero, O. L., Soto-García, L. L., Claeys, M., Kourtchev, I., Rissler, J., Swietlicki, E., Tagliavini, E., Schkolnik, G., Falkovich, A. H., Rudich, Y., Fisch, G. and Gatti, L. V~~:~~ Overview of the inorganic and organic composition of size-segregated aerosol in Rondônia, Brazil, from the biomass-burning period to the onset of the wet season, J. Geophys. Res., 112(D1), D01201, doi:10.1029/2005JD006741, 2007.

Gao, Y., Lai, S., Lee, S. C., Yau, P. S., Huang, Y., Cheng, Y., Wang, T., Xu, Z., Yuan, C. and Zhang, Y.: Optical properties of size-resolved particles at a Hong Kong urban site during winter, Atmos. Res., 155, 1–12, doi:10.1016/j.atmosres.2014.10.020, 2015.

Han, T., Qiao, L., Zhou, M., Qu, Y., Du, J., Liu, X., Lou, S., Chen, C., Wang, H., Zhang, F., Yu, Q. and Wu, Q.: Chemical and optical properties of aerosols and their interrelationship in winter in the megacity Shanghai of China, J. Environ. Sci. (China), 27(C), 59–69, doi:10.1016/j.jes.2014.04.018, 2015.

Hand, J. L. and Malm, W. C.: Review of aerosol mass scattering efficiencies from ground-based measurements since 1990, J. Geophys. Res. Atmos., 112(16), doi:10.1029/2007JD008484, 2007.

He, C., Liou, K. N., Takano, Y., Zhang, R., Levy Zamora, M., Yang, P., Li, Q. and Leung, L. R.: Variation of the radiative properties during black carbon aging: Theoretical and experimental intercomparison, Atmos. Chem. Phys., 15(20), 11967–11980, doi:10.5194/acp-15-11967-2015, 2015.

Formatted: Font color: Black

Formatted: Normal, Border: Top: (No border), Bottom: (N border), Left: (No border), Right: (No border), Between : (border), Tab stops: 3.13", Centered + 6.27", Right

Holanda, B. A., Pöhlker, M. L., Walter, D., Saturno, J., Sörgel, M., Ditas, J., Ditas, F., Schulz, C., Franco, M. A., Wang, Q., Donth, T., Artaxo, P., Barbosa, H. M. J., Borrmann, S., Braga, R., Brito, J., Cheng, Y., Dollner, M., Kaiser, J. W., Klimach, T., Knote, C., Krüger, O. O., Fütterer, D., Lavrič, J. V., Ma, N., Machado, L. A. T., Ming, J., Morais, F. G., Paulsen, H., Sauer, D., Schlager, H., Schneider, J., Su, H., Weinzierl, B., Walser, A., Wendisch, M., Ziereis, H., Zöger, M., Pöschl, U., Andreae, M. O. and Pöhlker, C.: Influx of African biomass burning aerosol during the Amazonian dry season through layered transatlantic transport of black carbon-rich smoke, Atmos. Chem. Phys., 20(8), 4757–4785, doi:10.5194/acp-20-4757-2020, 2020.

Holanda, B. A., Franco, M. A., Walter, D., Artaxo, P., Carbone, S., Cheng, Y., Chowdhury, S., Ditas, F., Gysel-Beer, M., Klimach, T., Kremper, L. A., Krüger, O. O., Lavric, J. V., Lelieveld, J., Ma, C., Machado, L. A. T., Modini, R. L., Morais, F. G., Pozzer, A., Saturno, J., Su, H., Wendisch, M., Wolff, S., Pöhlker, M. L., Andreae, M. O., Pöschl, U. and Pöhlker, C.: African biomass burning affects aerosol cycling over the Amazon, Commun. Earth Environ., 4(1), 1–15, doi:10.1038/s43247-023-00795-5, 2023.

Hu, W., Palm, B. B., Day, D. A., Campuzano-Jost, P., Krechmer, J. E., Peng, Z., De Sa Suzane, S., Martin, S. T., Alexander, M. L., Baumann, K., Hacker, L., Kiendler-Scharr, A., Koss, A. R., De Gouw, J. A., Goldstein, A. H., Seco, R., Sjostedt, S. J., Park, J. H., Guenther, A. B., Kim, S., Canonaco, F., Prévôt, A. S. H., Brune, W. H. and Jimenez, J. L.: Volatility and lifetime against OH heterogeneous reaction of ambient isoprene-epoxydiols-derived secondary organic aerosol (IEPOX-SOA), Atmos. Chem. Phys., 16(18), 11563–11580, doi:10.5194/acp-16-11563-2016, 2016.

Hu, W. W., Campuzano-Jost, P., Palm, B. B., Day, D. A., Ortega, A. M., Hayes, P. L., Krechmer, J. E., Chen, Q., Kuwata, M., Liu, Y. J., de Sá, S. S., Martin, S. T., Hu, M., Budisulistiorini, S. H., Riva, M., Surratt, J. D., St. Clair, J. M., Isaacman-Van Wertz, G., Yee, L. D., Goldstein, A. H., Carbone, S., Artaxo, P., de Gouw, J. A., Koss, A., Wisthaler, A., Mikoviny, T., Karl, T., Kaser, L., Jud, W., Hansel, A., Docherty, K. S., Robinson, N. H., Coe, H., Allan, J. D., Canagaratna, M. R., Paulot, F. and Jimenez, J. L.: Characterization of a real-time tracer for Isoprene Epoxydiols-derived Secondary Organic Aerosol (IEPOX-SOA) from aerosol mass spectrometer measurements, Atmos. Chem. Phys. Discuss., 15(8), 11223–11276, doi:10.5194/acpd-15-11223-2015, 2015.

Instituto Nacional de Pesquisas Espaciais: Portal do Monitoramento de Queimadas e Incêndios Florestais, [online] Available from: http://terrabrasilis.dpi.inpe.br/queimadas/situacao-atual/estatisticas/estatisticas_estados/#afooter, 2024.

Jimenez, J. L., Canagaratna, M. R., Donahue, N. M., Prevot, a. S. H., Zhang, Q., Kroll, J. H., DeCarlo, P. F., Allan, J. D., Coe, H., Ng, N. L., Aiken, a. C., Docherty, K. S., Ulbrich, I. M., Grieshop, a. P., Robinson, a. L., Duplissy, J., Smith, J. D., Wilson, K. R., Lanz, V. a., Hueglin, C., Sun, Y. L., Tian, J., Laaksonen, A., Raatikainen, T., Rautiainen, J., Vaattovaara, P., Ehn, M., Kulmala, M., Tomlinson, J. M., Collins, D. R., Cubison, M. J., Dunlea, J., Huffman, J. a., Onasch, T. B., Alfarra, M. R., Williams, P. I., Bower, K., Kondo, Y., Schneider, J., Drewnick, F., Borrmann, S., Weimer, S., Demerjian, K., Salcedo, D., Cottrell, L., Griffin, R., Takami, A., Miyoshi, T., Hatakeyama, S., Shimono, A., Sun, J. Y., Zhang, Y. M., Dzepina, K., Kimmel, J. R., Sueper, D., Jayne, J. T., Herndon, S. C., Trimborn, a. M., Williams, L. R., Wood, E. C., Middlebrook, a. M., Kolb, C. E., Baltensperger, U. and Worsnop, D. R.: Evolution of Organic Aerosols in the Atmosphere, Science (80-.)., 326(5959), 1525–1529, doi:10.1126/science.1180353, 2009.

Jing, J., Wu, Y., Tao, J., Che, H., Xia, X., Zhang, X., Yan, P., Zhao, D. and Zhang, L.: Observation and analysis of near-surface atmospheric aerosol optical properties in urban Beijing, Particuology, 18, 144–154, doi:10.1016/j.partic.2014.03.013, 2015.

Kim, K. W.: Optical properties of size-resolved aerosol chemistry and visibility variation observed in the urban site of seoul, korea, Aerosol Air Qual. Res., 15(1), 271–283, doi:10.4209/aaqr.2013.11.0347, 2015.

Kleinman, L. I., Sedlacek, A. J., Adachi, K., Buseck, P. R., Collier, S., Dubey, M. K., Hodshire, A. L., Lewis, E., Onasch, T. B., Pierce, J. R., Shilling, J., Springston, S. R., Wang, J., Zhang, Q., Zhou, S. and Yokelson, R. J.: Rapid evolution of aerosol particles and their optical properties downwind of wildfires in the western US, Atmos. Chem. Phys., 20(21), 13319–13341, doi:10.5194/acp-20-13319-2020, 2020.

Kroll, J. H., Ng, N. L., Murphy, S. M., Flagan, R. C. and Seinfeld, J. H.: Secondary Organic Aerosol Formation from Isoprene Photooxidation, Environ. Sci. Technol., 40(6), 1869–1877, doi:10.1021/es0524301, 2006.

Kuhn, U., Ganzeveld, L., Thielmann, A., Dindorf, T., Schebeske, G., Welling, M., Sciare, J., Roberts, G., Meixner, F. X., Kesselmeier, J., Lelieveld, J., Kolle, O., Ciccioli, P., Lloyd, J., Trentmann, J., Artaxo, P. and Andreae, M. O.: Impact of Manaus City on the Amazon Green Ocean atmosphere: Ozone production, precursor sensitivity and aerosol load, Atmos. Chem. Phys., 10(19), 9251–9282, doi:10.5194/acp-10-9251-2010, 2010.

Laskin, A., Laskin, J. and Nizkorodov, S. A.: Chemistry of Atmospheric Brown Carbon, Chem. Rev., 115(10), 4335–4382,

Formatted: Font color: Black

Formatted: Normal, Border: Top: (No border), Bottom: (N border), Left: (No border), Right: (No border), Between : (border), Tab stops: 3.13", Centered + 6.27", Right

doi:10.1021/cr5006167, 2015.

Lee, T., Sullivan, A. P., Mack, L., Jimenez, J. L., Kreidenweis, S. M., Onasch, T. B., Worsnop, D. R., Malm, W., Wold, C. E., Hao, W. M. and Collett, J. L.: Chemical Smoke Marker Emissions During Flaming and Smoldering Phases of Laboratory Open Burning of Wildland Fuels, Aerosol Sci. Technol., 44(9), i–v, doi:10.1080/02786826.2010.499884, 2010.

Levin, E. J. T., McMeeking, G. R., Carrico, C. M., Mack, L. E., Kreidenweis, S. M., Wold, C. E., Moosmüller, H., Arnott, W. P., Hao, W. M., Collett, J. L. and Malm, W. C.: Biomass burning smoke aerosol properties measured during Fire Laboratory at Missoula Experiments (FLAME), J. Geophys. Res. Atmos., 115(18), 1–15, doi:10.1029/2009JD013601, 2010.

Li, W., Riemer, N., Xu, L., Wang, Y., Adachi, K., Shi, Z., Zhang, D., Zheng, Z. and Laskin, A.: Microphysical properties of atmospheric soot and organic particles: measurements, modeling, and impacts, npj Clim. Atmos. Sci., 7(1), 65, doi:10.1038/s41612-024-00610-8, 2024.

Lin, Y. H., Zhang, Z., Docherty, K. S., Zhang, H., Budisulistiorini, S. H., Rubitschun, C. L., Shaw, S. L., Knipping, E. M., Edgerton, E. S., Kleindienst, T. E., Gold, A. and Surratt, J. D.: Isoprene ~~Epoxydiols~~epoxydiols as ~~Precursors~~precursors to ~~Secondary Organic Aerosol Formation~~ secondary organic aerosol formation: Acid-~~Catalyzed Reactive Uptake Studies~~catalyzed reactive uptake studies with ~~Authentic Compounds, ~~,authentic compounds, Environ. Sci. Technol., 46(1), 250–258, doi:10.1021/es202554c, 2012.

Luo, J., Zhang, Y. and Zhang, Q.: The Ångström Exponent and Single-Scattering Albedo of Black Carbon: Effects of Different Coating Materials, Atmosphere (Basel)., 11(10), 1103, doi:10.3390/atmos11101103, 2020.

Ma, N., Zhao, C. S., Nowak, A., Müller, T., Pfeifer, S., Cheng, Y. F., Deng, Z. Z., Liu, P. F., Xu, W. Y., Ran, L., Yan, P., Göbel, T., Hallbauer, E., Mildenberger, K., Henning, S., Yu, J., Chen, L. L., Zhou, X. J., Stratmann, F. and Wiedensohler, A.: Aerosol optical properties in the North China Plain during HaChi campaign: An in-situ optical closure study, Atmos. Chem. Phys., 11(12), 5959–5973, doi:10.5194/acp-11-5959-2011, 2011.

Malm, W. C., Day, D. E., Carrico, C., Kreidenweis, S. M., Collett, J. L., McMeeking, G., Lee, T., Carrillo, J. and Schichtel, B.: Intercomparison and closure calculations using measurements of aerosol species and optical properties during the Yosemite aerosol characterization study, J. Geophys. Res. D Atmos., 110(14), 1–21, doi:10.1029/2004JD005494, 2005.

Marais, E. A., Jacob, D. J., Jimenez, J. L., Campuzano-Jost, P., Day, D. A., Hu, W., Krechmer, J., Zhu, L., Kim, P. S., Miller, C. C., Fisher, J. A., Travis, K., Yu, K., Hanisco, T. F., Wolfe, G. M., Arkinson, H. L., Pye, H. O. T., Froyd, K. D., Liao, J. and McNeill, V. F.: Aqueous-phase mechanism for secondary organic aerosol formation from isoprene: application to the southeast United States and co-benefit of SO2 emission controls, Atmos. Chem. Phys., 16(3), 1603–1618, doi:10.5194/acp-16-1603-2016, 2016.

~~Marengo, J. A., Liebmann, B., Kousky, V. E., Filizola, N. P. and Wainer, I. C.: Onset and End of the Rainy Season in the Brazilian Amazon Basin, J. Clim., 14(5), 833–852, doi:10.1175/1520-0442(2001)014<0833:OAEOTR>2.0.CO;2, 2001.~~

Martin, S. T., Andreae, M. O., Althausen, D., Artaxo, P., Baars, H., Borrmann, S., Chen, Q., Farmer, D. K., Guenther, a., Gunthe, S. S., Jimenez, J. L., Karl, T., Longo, K., Manzi, a., Müller, T., Pauliquevis, T., Petters, M. D., Prenni, a. J., Pöschl, U., Rizzo, L. V., Schneider, J., Smith, J. N., Swietlicki, E., Tota, J., Wang, J., Wiedensohler, a. and Zorn, S. R.: An overview of the Amazonian Aerosol Characterization Experiment 2008 (AMAZE-08), Atmos. Chem. Phys., 10(23), 11415–11438, doi:10.5194/acp-10-11415-2010, 2010a.

Martin, S. T., Andreae, M. O., Artaxo, P., Baumgardner, D., Chen, Q., Goldstein, A. H., Guenther, A., Heald, C. L., Mayol-Bracero, O. L., McMurry, P. H., Pauliquevis, T., Pöschl, U., Prather, K. A., Roberts, G. C., Saleska, S. R., Silva Dias, M. A., Spracklen, D. V, Swietlicki, E. and Trebs, I.: Sources and properties of Amazonian aerosol particles, Rev. Geophys., 48(2), RG2002, doi:10.1029/2008RG000280, 2010b.

Martin, S. T., Artaxo, P., Machado, L. A. T., Manzi, A. O., Souza, R. A. F., Schumacher, C., Wang, J., Andreae, M. O., Barbosa, H. M. J., Fan, J., Fisch, G., Goldstein, A. H., Guenther, A., Jimenez, J. L., Pöschl, U., Silva Dias, M. A., Smith, J. N. and Wendisch, M.: Introduction: Observations and Modeling of the Green Ocean Amazon (GoAmazon2014/5), Atmos. Chem. Phys. Discuss., 15(21), 30175–30210, doi:10.5194/acpd-15-30175-2015, 2015.

Metcalf, A. R., Loza, C. L., Coggon, M. M., Craven, J. S., Jonsson, H. H., Flagan, R. C. and Seinfeld, J. H.: Secondary organic aerosol coating formation and evaporation: Chamber studies using black carbon seed aerosol and the single-particle soot photometer, Aerosol Sci. Technol., 47(3), 326–347, doi:10.1080/02786826.2012.750712, 2013.

Formatted: Font color: Black

Formatted: Normal, Border: Top: (No border), Bottom: (N border), Left: (No border), Right: (No border), Between : (border), Tab stops: 3.13", Centered + 6.27", Right

Middlebrook, A. M., Bahreini, R., Jimenez, J. L. and Canagaratna, M. R.: Evaluation of Composition-Dependent Collection Efficiencies for the Aerodyne Aerosol Mass Spectrometer using Field Data, Aerosol Sci. Technol., 46(3), 258–271, doi:10.1080/02786826.2011.620041, 2012.

Müller, T., Henzing, J. S., De Leeuw, G., Wiedensohler, A., Alastuey, A., Angelov, H., Bizjak, M., Collaud Coen, M., Engström, J. E., Gruening, C., Hillamo, R., Hoffer, A., Imre, K., Ivanow, P., Jennings, G., Sun, J. Y., Kalivitis, N., Karlsson, H., Komppula, M., Laj, P., Li, S. M., Lunder, C., Marinoni, A., Martins Dos Santos, S., Moerman, M., Nowak, A., Ogren, J. A., Petzold, A., Pichon, J. M., Rodriquez, S., Sharma, S., Sheridan, P. J., Teinilä, K., Tuch, T., Viana, M., Virkkula, A., Weingartner, E., Wilhelm, R. and Wang, Y. Q.: Characterization and intercomparison of aerosol absorption photometers: Result of two intercomparison workshops, Atmos. Meas. Tech., 4(2), 245–268, doi:10.5194/amt-4-245-2011, 2011.

~~Myhre, G., Samset, B. H., Schulz, M., Balkanski, Y., Bauer, S., Berntsen, T. K., Bian, H., Bellouin, N., Chin, M., Diehl, T., Easter, R. C., Feichter, J., Ghan, S. J., Hauglustaine, D., Iversen, T., Kinne, S., Kirkeväg, A., Lamarque, J. F., Lin, G., Liu, X., Lund, M. T., Luo, G., Ma, X., Van Noije, T., Penner, J. E., Rasch, P. J., Ruiz, A., Seland, Skeie, R. B., Stier, P., Takemura, T., Tsigaridis, K., Wang, P., Wang, Z., Xu, L., Yu, H., Yu, F., Yoon, J. H., Zhang, K., Zhang, H. and Zhou, C.: Radiative forcing of the direct aerosol effect from AeroCom Phase II simulations, Atmos. Chem. Phys., 13(4), 1853–1877, doi:10.5194/acp-13-1853-2013, 2013.~~

Nah, T., Xu, L., Osborne-Benthaus, K. A., White, S. M., France, S. and Lee Ng, N.: Mixing order of sulfate aerosols and isoprene epoxydiols affects secondary organic aerosol formation in chamber experiments, Atmos. Environ., 217(September), doi:10.1016/j.atmosenv.2019.116953, 2019.

Nakayama, T., Hagino, R., Matsumi, Y., Sakamoto, Y., Kawasaki, M., Yamazaki, A., Uchiyama, A., Kudo, R., Moteki, N., Kondo, Y. and Tonokura, K.: Measurements of aerosol optical properties in central Tokyo during summertime using cavity ring-down spectroscopy: Comparison with conventional techniques, Atmos. Environ., 44(25), 3034–3042, doi:10.1016/j.atmosenv.2010.05.008, 2010.

Nascimento, J. P., Bela, M. M., Meller, B. B., Banducci, A. L., Rizzo, L. V., Liduvino Vara-Vela, A., Barbosa, H. M. J., Gomes, H., Rafee, S. A. A., Franco, M. A., Carbone, S., Cirino, G. G., Souza, R. A. F., Mckeen, S. A. and Artaxo, P.: Aerosols from anthropogenic and biogenic sources and their interactions-modeling aerosol formation, optical properties, and impacts over the central Amazon basin, Atmos. Chem. Phys., 21(9), 6755–6779, doi:10.5194/acp-21-6755-2021, 2021.

Ng, N. L., Herndon, S. C., Trimborn, A., Canagaratna, M. R., Croteau, P. L., Onasch, T. B., Sueper, D., Worsnop, D. R., Zhang, Q., Sun, Y. L. and Jayne, J. T.: An Aerosol Chemical Speciation Monitor (ACSM) for routine monitoring of the composition and mass concentrations of ambient aerosol, Aerosol Sci. Technol., 45(7), 780–794, doi:10.1080/02786826.2011.560211, 2011.

Paatero, P. and Tapper, U.: Positive Matrix Factorization: a non-negative factor model with optimal utilization of error estimates of data values, Environmetrics, 5, 111–126, 1994.

Palácios, R. da S., Romera, K. S., Curado, L. F. A., Banga, N. M., Rothmund, L. D., Sallo, F. da S., Morais, D., Santos, A. C. A., Moraes, T. J., Morais, F. G., Landulfo, E., Franco, M. A. de M., Kuhnen, I. A., Marques, J. B., Nogueira, J. de S., Júnior, L. C. G. D. V. and Rodrigues, T. R.: Long term analysis of optical and radiative properties of aerosols in the amazon basin, Aerosol Air Qual. Res., 20(1), 139–154, doi:10.4209/aaqr.2019.04.0189, 2020.

~~Paredes-Miranda, G., Arnott, W. P., Jimenez, J. L., Aiken, A. C., Gaffney, J. S. and Marley, N. A.: Primary and secondary contributions to aerosol light scattering and absorption in Mexico City during the MILAGRO 2006 campaign, Atmos. Chem. Phys., 9(11), 3721–3730, doi:10.5194/acp-9-3721-2009, 2009.~~

Palm, B. B., De Sá, S. S., Day, D. A., Campuzano-Jost, P., Hu, W., Seco, R., Sjostedt, S. J., Park, J. H., Guenther, A. B., Kim, S., Brito, J., Wurm, F., Artaxo, P., Thalman, R., Wang, J., Yee, L. D., Wernis, R., Isaacman-VanWertz, G., Goldstein, A. H., Liu, Y., Springston, S. R., Souza, R., Newburn, M. K., Lizabeth Alexander, M., Martin, S. T. and Jimenez, J. L.: Secondary organic aerosol formation from ambient air in an oxidation flow reactor in central Amazonia, Atmos. Chem. Phys., 18(1), 467–493, doi:10.5194/acp-18-467-2018, 2018.

Pani, S. K., Lin, N. H., Wang, S. H., Chantara, S., Griffith, S. M. and Chang, J. H. W.: Aerosol mass scattering efficiencies and single scattering albedo under high mass loading in Chiang Mai valley, Thailand, Atmos. Environ., 308(April), 119867, doi:10.1016/j.atmosenv.2023.119867, 2023.

Park, S., Kim, S. W., Lin, N. H., Pani, S. K., Sheridan, P. J. and Andrews, E.: Variability of aerosol optical properties observed at a polluted

Formatted: Font color: Black

Formatted: Normal, Border: Top: (No border), Bottom: (N border), Left: (No border), Right: (No border), Between : (border), Tab stops: 3.13", Centered + 6.27", Right

marine (Gosan, korea) and a high-altitude mountain (Lulin, Taiwan) site in the asian continental outflow, Aerosol Air Qual. Res., 19(6), 1272–1283, doi:10.4209/aaqr.2018.11.0416, 2019.

Petzold, A., Schloesser, H., Sheridan, P. J., Arnott, W. P., Ogren, J. A. and Virkkula, A.: Evaluation of Multiangle Absorption Photometry for Measuring Aerosol Light Absorption, Aerosol Sci. Technol., 39(1), 40–51, doi:10.1080/027868290901945, 2005.

~~Pohlker, C., Wiedemann, K. T., Sinha, B., Shiraiwa, M., Gunthe, S. S., Smith, M., Su, H., Artaxo, P., Chen, Q., Cheng, Y., Elbert, W., Gilles, M. K., Kilcoyne, A. L. D., Moffet, R. C., Weigand, M., Martin, S. T., Poschl, U., Andreae, M. O.,~~ Pitchford, M., Malm, W., Schichtel, B., Kumar, N., Lowenthal, D. and Hand, J.: Revised algorithm for estimating light extinction from IMPROVE particle speciation data, J. Air Waste Manag. Assoc., 57(11), 1326–1336, doi:10.3155/1047-3289.57.11.1326, 2007.

Pöhlker, C., Wiedemann, K. T., Sinha, B., Shiraiwa, M., Gunthe, S. S., Smith, M., Su, H., Artaxo, P., Chen, Q., Cheng, Y., Elbert, W., Gilles, M. K., Kilcoyne, A. L. D., Moffet, R. C., Weigand, M., Martin, S. T., Pöschl, U. and Andreae, M. O.: Biogenic ~~potassium salt particles~~Potassium Salt Particles as ~~seeds~~Seeds for ~~secondary organic aerosol~~Secondary Organic Aerosol in the Amazon~~.~~, Science~~.~~ (80-.)., 337(6098), 1075–~~8~~1078, doi:10.1126/science.1223264, 2012.

~~Pöhlker, M. L., Pöhlker, C., Ditas, F., Klimach, T., De Angelis, I. H., Araújo, A., Brito, J., Carbone, S., Cheng, Y., Chi, X., Ditz, R., Gunthe, S. S., Kesselmeier, J., Könemann, T., Lavrič, J. V., Martin, S. T., Mikhailov, E., Moran-Zuloaga, D., Rose, D., Saturno, J., Su, H., Thalman, R., Walter, D., Wang, J., Wolff, S., Barbosa, H. M. J., Artaxo, P., Andreae, M. O. and Pöschl, U.: Long-term observations of cloud condensation nuclei in the Amazon rain forest - Part 1: Aerosol size distribution, hygroscopicity, and new model parametrizations for CCN prediction, Atmos. Chem. Phys., 16(24), 15709–15740, doi:10.5194/acp-16-15709-2016, 2016.~~

Pöhlker, M. L., Ditas, F., Saturno, J., Klimach, T., Hrabě De Angelis, I., Araùjo, A. C., Brito, J., Carbone, S., Cheng, Y., Chi, X., Ditz, R., Gunthe, S. S., Holanda, B. A., Kandler, K., Kesselmeier, J., Könemann, T., Krüger, O. O., Lavric, J. V., Martin, S. T., Mikhailov, E., Moran-Zuloaga, D., Rizzo, L. V., Rose, D., Su, H., Thalman, R., Walter, D., Wang, J., Wolff, S., Barbosa, H. M. J., Artaxo, P., Andreae, M. O., Pöschl, U. and Pöhlker, C.: Long-term observations of cloud condensation nuclei over the Amazon rain forest - Part 2: Variability and characteristics of biomass burning, long-range transport, and pristine rain forest aerosols, Atmos. Chem. Phys., 18(14), 10289–10331, doi:10.5194/acp-18-10289-2018, 2018.

Ponczek, M., Franco, M. A., Carbone, S., Rizzo, L. V., Monteiro dos Santos, D., Morais, F. G., Duarte, A., Barbosa, H. M. J. and Artaxo, P.: Linking the chemical composition and optical properties of biomass burning aerosols in Amazonia, Environ. Sci. Atmos., 2(2), 252–269, doi:10.1039/d1ea00055a, 2021.

Pöschl, U., Martin, S. T., Sinha, B., Chen, Q., Gunthe, S. S., Huffman, J. A., Borrmann, S., Farmer, D. K., Garland, R. M., Helas, G., Jimenez, J. L., King, S. M., Manzi, A., Mikhailov, E., Pauliquevis, T., Petters, M. D., Prenni, A. J., Roldin, P., Rose, D., Schneider, J., Su, H., Zorn, S. R., Artaxo, P. and Andreae, M. O.: Rainforest Aerosols as Biogenic Nuclei of Clouds and Precipitation in the Amazon, Science (80-.)., 329(5998), 1513–1516, doi:10.1126/science.1191056, 2010.

Ram, K., Singh, S., Sarin, M. M., Srivastava, A. K. and Tripathi, S. N.: Variability in aerosol optical properties over an urban site, Kanpur, in the Indo-Gangetic Plain: A case study of haze and dust events, Atmos. Res., 174–175, 52–61, doi:10.1016/j.atmosres.2016.01.014, 2016.

Reid, J. S., ~~Koppmann, R.,~~ Eck, T. F~~. and .~~, Christopher, S. A., Koppman, R., Dubovik, O., Eleuterio, D. P., Holben, B. N., Reid, E. A. and Zhang, J.: A review of biomass burning emissions part ~~II: intensive physical~~III: Intensive optical properties of biomass burning particles, Atmos. Chem. Phys., 5(3), ~~799–825~~827–849, doi:10.5194/acp-5-~~799~~827-2005, 2005.

Rizzo, L. V., Artaxo, P., Müller, T., Wiedensohler, A., Paixão, M., Cirino, G. G., Arana, A., Swietlicki, E., Roldin, P., Fors, E. O., Wiedemann, K. T., Leal, L. S. M. and Kulmala, M.: Long term measurements of aerosol optical properties at a primary forest site in Amazonia, Atmos. Chem. Phys., 13(5), 2391–2413, doi:10.5194/acp-13-2391-2013, 2013.

Romshoo, B., Müller, T., Pfeifer, S., Saturno, J., Nowak, A., Ciupek, K., Quincey, P. and Wiedensohler, A.: Optical properties of coated black carbon aggregates: Numerical simulations, radiative forcing estimates, and size-resolved parameterization scheme, Atmos. Chem. Phys., 21(17), 12989–13010, doi:10.5194/acp-21-12989-2021, 2021.

de Sá, S. S., Palm, B. B., Campuzano-Jost, P., Day, D. A., Newburn, M. K., Hu, W., Isaacman-VanWertz, G., Yee, L. D., Thalman, R., Brito, J., Carbone, S., Artaxo, P., Goldstein, A. H., Manzi, A. O., Souza, R. A. F., Mei, F., Shilling, J. E., Springston, S. R., Wang, J., Surratt, J. D., Alexander, M. L., Jimenez, J. L. and Martin, S. T.: Influence of urban pollution on the production of organic particulate matter from

Formatted: Font color: Black

Formatted: Normal, Border: Top: (No border), Bottom: (N border), Left: (No border), Right: (No border), Between : (border), Tab stops: 3.13", Centered + 6.27", Right

isoprene epoxydiols in central Amazonia, Atmos. Chem. Phys., 17(11), 6611–6629, doi:10.5194/acp-17-6611-2017, 2017.

de Sá, S. S., ~~Palm, B. B., Campuzano-Jost, P., Day, D. A., Hu, W., Isaacman-VanWertz, G., Yee, L. D., Brito, J., Carbone, S., Ribeiro, I. O., Cirino, G. G., Liu, Y., Thalman, R., Sedlacek, A., Funk, A., Schumacher, C., Shilling, J. E., Schneider, J., Artaxo, P., Goldstein, A. H., Souza, R. A. F., Wang, J., McKinney, K. A., Barbosa, H., Alexander, M. L., Jimenez, J. L. and Martin, S. T.: Urban influence on the concentration and composition of submicron particulate matter in central Amazonia, Atmos. Chem. Phys., 18(16), 12185–12206, doi:10.5194/acp-18-12185-2018, 2018.~~

~~de Sá, S. S.,~~ Rizzo, L. V., Palm, B. B., Campuzano-Jost, P., Day, D. A., Yee, L. D., Wernis, R., Isaacman-VanWertz, G., Brito, J., Carbone, S., Liu, Y. J., Sedlacek, A., Springston, S., Goldstein, A. H., Barbosa, H. M. J., Alexander, M. L., Artaxo, P., Jimenez, J. L. and Martin, S. T.: Contributions of biomass-burning, urban, and biogenic emissions to the concentrations and light-absorbing properties of particulate matter in central Amazonia during the dry season, Atmos. Chem. Phys., 19(12), 7973–8001, doi:10.5194/acp-19-7973-2019, 2019.

Saide, P. E., Thapa, L. H., Ye, X., Pagonis, D., Campuzano-Jost, P., Guo, H., Schuneman, M. L., Jimenez, J. L., Moore, R., Wiggins, E., Winstead, E., Robinson, C., Thornhill, L., Sanchez, K., Wagner, N. L., Ahern, A., Katich, J. M., Perring, A. E., Schwarz, J. P., Lyu, M., Holmes, C. D., Hair, J. W., Fenn, M. A. and Shingler, T. J.: Understanding the Evolution of Smoke Mass Extinction Efficiency Using Field Campaign Measurements, Geophys. Res. Lett., 49(18), 1–12, doi:10.1029/2022GL099175, 2022.

Saturno, J., Ditas, F., De Vries, M. P., Holanda, B. A., Pöhlker, M. L., Carbone, S., Walter, D., Bobrowski, N., Brito, J., Chi, X., Gutmann, A., De Angelis, I. H., Machado, L. A. T., Moran-Zuloaga, D., Rüdiger, J., Schneider, J., Schulz, C., Wang, Q., Wendisch, M., Artaxo, P., Wagner, T., Pöschl, U., Andreae, M. O. and Pöhlker, C.: African volcanic emissions influencing atmospheric aerosols over the Amazon rain forest, Atmos. Chem. Phys., 18(14), 10391–10405, doi:10.5194/acp-18-10391-2018, 2018a.

Saturno, J., Holanda, B. A., Pöhlker, C., Ditas, F., Wang, Q., Moran-Zuloaga, D., Brito, J., Carbone, S., Cheng, Y., Chi, X., Ditas, J., Hoffmann, T., Hrabe De Angelis, I., Könemann, T., Lavrič, J. V., Ma, N., Ming, J., Paulsen, H., Pöhlker, M. L., Rizzo, L. V., Schlag, P., Su, H., Walter, D., Wolff, S., Zhang, Y., Artaxo, P., Pöschl, U. and Andreae, M. O.: Black and brown carbon over central Amazonia: Long-term aerosol measurements at the ATTO site, Atmos. Chem. Phys., 18(17), 12817–12843, doi:10.5194/acp-18-12817-2018, 2018b.

Schuster, G. L., Dubovik, O. and Holben, B. N.: Angstrom exponent and bimodal aerosol size distributions, J. Geophys. Res. Atmos., 111(D7), D07207, doi:10.1029/2005JD006328, 2006.

Schwarz, J. P., Gao, R. S., Fahey, D. W., Thomson, D. S., Watts, L. A., Wilson, J. C., Reeves, J. M., Darbeheshti, M., Baumgardner, D. G., Kok, G. L., Chung, S. H., Schulz, M., Hendricks, J., Lauer, A., Kärcher, B., Slowik, J. G., Rosenlof, K. H., Thompson, T. L., Langford, A. O., Loewenstein, M. and Aikin, K. C.: Single-particle measurements of midlatitude black carbon and light-scattering aerosols from the boundary layer to the lower stratosphere, J. Geophys. Res. Atmos., 111(16), 1–15, doi:10.1029/2006JD007076, 2006.

Sena, E. T., Artaxo, P. and Correia, a. L.: Spatial variability of the direct radiative forcing of biomass burning aerosols and the effects of land use change in Amazonia, Atmos. Chem. Phys., 13(3), 1261–1275, doi:10.5194/acp-13-1261-2013, 2013.

Shrivastava, M., Andreae, M. O., Artaxo, P., Barbosa, H. M. J., Berg, L. K., Brito, J., Ching, J., Easter, R. C., Fan, J., Fast, J. D., Feng, Z., Fuentes, J. D., Glasius, M., Goldstein, A. H., Alves, E. G., Gomes, H., Gu, D., Guenther, A., Jathar, S. H., Kim, S., Liu, Y., Lou, S., Martin, S. T., McNeill, V. F., Medeiros, A., de Sá, S. S., Shilling, J. E., Springston, S. R., Souza, R. A. F., Thornton, J. A., Isaacman-VanWertz, G., Yee, L. D., Ynoue, R., Zaveri, R. A., Zelenyuk, A. and Zhao, C.: Urban pollution greatly enhances formation of natural aerosols over the Amazon rainforest, Nat. Commun., 10(1), doi:10.1038/s41467-019-08909-4, 2019.

~~Smith, D. M., Fiddler, M. N., Pokhrel, R. P. and Bililign, S.: Laboratory studies of fresh and aged biomass burning aerosol emitted from east African biomass fuels-Part 1: Optical properties, Atmos. Chem. Phys., 20(17), 10149–10168, doi:10.5194/acp-20-10149-2020, 2020.~~

Soni, K., Singh, S., Bano, T., Tanwar, R. S., Nath, S. and Arya, B. C.: Variations in single scattering albedo and Angstrom absorption exponent during different seasons at Delhi, India, Atmos. Environ., 44(35), 4355–4363, doi:10.1016/j.atmosenv.2010.07.058, 2010.

Sun, J., Zhang, Q., Canagaratna, M. R., Zhang, Y., Ng, N. L., Sun, Y., Jayne, J. T., Zhang, X., Zhang, X. and Worsnop, D. R.: Highly time- and size-resolved characterization of submicron aerosol particles in Beijing using an Aerodyne Aerosol Mass Spectrometer, Atmos. Environ., 44(1), 131–140, doi:10.1016/j.atmosenv.2009.03.020, 2010.

Surratt, J. D., Chan, A. W. H., Eddingsaas, N. C., Chan, M., Loza, C. L., Kwan, A. J., Hersey, S. P., Flagan, R. C., Wennberg, P. O. and

Formatted: Font color: Black

Formatted: Normal, Border: Top: (No border), Bottom: (N border), Left: (No border), Right: (No border), Between : (border), Tab stops: 3.13", Centered + 6.27", Right

Seinfeld, J. H.: Reactive intermediates revealed in secondary organic aerosol formation from isoprene, Proc. Natl. Acad. Sci., 107(15), 6640–6645, doi:10.1073/pnas.0911114107, 2010.

Szopa, S., Naik, V., Artaxo, P., Berntsen, T., Collins, W. D., Fuzzi, S., Gallardo, L., Kiendler-Scharr, A., Klimont, Z., Liao, H., Unger, N. and Zanis, P.: Short-lived Climate Forcers, in Climate Change 2021 – The Physical Science Basis, pp. 817–922, Cambridge University Press., 2023.

Tao, J., Zhang, Z., Wu, Y., Zhang, L., Wu, Z., Cheng, P., Li, M., Chen, L., Zhang, R. and Cao, J.: Impact of particle number and mass size distributions of major chemical components on particle mass scattering efficiency in urban Guangzhou in southern China, Atmos. Chem. Phys., 19(13), 8471–8490, doi:10.5194/acp-19-8471-2019, 2019.

Tasoglou, A., Saliba, G., Subramanian, R. and Pandis, S. N.: Absorption of chemically aged biomass burning carbonaceous aerosol, J. Aerosol Sci., 113(April), 141–152, doi:10.1016/j.jaerosci.2017.07.011, 2017.

Tian, J., Wang, Q., Liu, H., Ma, Y., Liu, S., Zhang, Y., Ran, W., Han, Y. and Cao, J.: Measurement report: The importance of biomass burning in light extinction and direct radiative effect of urban aerosol during the COVID-19 lockdown in Xi'an, China, Atmos. Chem. Phys., 22(12), 8369–8384, doi:10.5194/acp-22-8369-2022, 2022.

Titos, G., Foyo-Moreno, I., Lyamani, H., Querol, X., Alastuey, A. and Alados-Arboledas, L.: Optical properties and chemical composition of aerosol particles at an urban location: An estimation of the aerosol mass scattering and absorption efficiencies, J. Geophys. Res. Atmos., 117(4), 1–12, doi:10.1029/2011JD016671, 2012.

Tuch, T. M., Haudek, A., Müller, T., Nowak, A., Wex, H. and Wiedensohler, A.: Design and performance of an automatic regenerating adsorption aerosol dryer for continuous operation at monitoring sites, Atmos. Meas. Tech., 2(2), 417–422, doi:10.5194/amt-2-417-2009, 2009.

Ulbrich, I. M., Canagaratna, M. R., Zhang, Q., Worsnop, D. R. and Jimenez, J. L.: Interpretation of organic components from Positive Matrix Factorization of aerosol mass spectrometric data, Atmos. Chem. Phys., 9(9), 2891–2918, doi:10.5194/acp-9-2891-2009, 2009.

Velazquez-Garcia, A., Crumeyrolle, S., de Brito, J. F., Tison, E., Bourrianne, E., Chiapello, I. and Riffault, V.: Deriving composition-dependent aerosol absorption, scattering and extinction mass efficiencies from multi-annual high time resolution observations in Northern France, Atmos. Environ., 298(December 2022), 119613, doi:10.1016/j.atmosenv.2023.119613, 2023.

Virtanen, P., Gommers, R., Oliphant, T. E., Haberland, M., Reddy, T., Cournapeau, D., Burovski, E., Peterson, P., Weckesser, W., Bright, J., van der Walt, S. J., Brett, M., Wilson, J., Millman, K. J., Mayorov, N., Nelson, A. R. J., Jones, E., Kern, R., Larson, E., Carey, C. J., Polat, İ., Feng, Y., Moore, E. W., VanderPlas, J., Laxalde, D., Perktold, J., Cimrman, R., Henriksen, I., Quintero, E. A., Harris, C. R., Archibald, A. M., Ribeiro, A. H., Pedregosa, F., van Mulbregt, P., Vijaykumar, A., Bardelli, A. Pietro, Rothberg, A., Hilboll, A., Kloeckner, A., Scopatz, A., Lee, A., Rokem, A., Woods, C. N., Fulton, C., Masson, C., Häggström, C., Fitzgerald, C., Nicholson, D. A., Hagen, D. R., Pasechnik, D. V., Olivetti, E., Martin, E., Wieser, E., Silva, F., Lenders, F., Wilhelm, F., Young, G., Price, G. A., Ingold, G.-L., Allen, G. E., Lee, G. R., Audren, H., Probst, I., Dietrich, J. P., Silterra, J., Webber, J. T., Slavič, J., Nothman, J., Buchner, J., Kulick, J., Schönberger, J. L., de Miranda Cardoso, J. V., Reimer, J., Harrington, J., Rodríguez, J. L. C., Nunez-Iglesias, J., Kuczynski, J., Tritz, K., Thoma, M., Newville, M., Kümmerer, M., Bolingbroke, M., Tartre, M., Pak, M., Smith, N. J., Nowaczyk, N., Shebanov, N., Pavlyk, O., Brodtkorb, P. A., Lee, P., McGibbon, R. T., Feldbauer, R., Lewis, S., Tygier, S., Sievert, S., Vigna, S., Peterson, S., More, S., Pudlik, T., et al.: SciPy 1.0: fundamental algorithms for scientific computing in Python, Nat. Methods, 17(3), 261–272, doi:10.1038/s41592-019-0686-2, 2020.

Wang, ~~Y.~~ H., ~~Liu, Z. R~~Shi, G., Tian, M., Zhang, ~~J. K., Hu, B., Ji, D. S., Yu, Y. C.~~L., Chen, Y., Yang, F. and ~~Wang, Y. S~~Cao, X.: Aerosol ~~physicochemical~~optical properties and ~~implications for visibility during an intense haze episode during winter~~chemical composition apportionment in ~~Beijing, Atmos. Chem. Phys., 15(6), 3205–3215~~Sichuan Basin, China, Sci. Total Environ., 577, 245–257, doi:10.~~5194/acp-15-3205-2015, 2015~~1016/j.scitotenv.2016.10.173, 2017.

Wang, Q., Sun, Y., Jiang, Q., Du, W., Sun, C., Fu, P. and Wang, Z.: Chemical composition of aerosol particles and light extinction apportionment before and during the heating season in Beijing, China, J. Geophys. Res. Atmos., 120(24), 12708–12722, doi:10.1002/2015JD023871, 2015.

Wang, Q., Saturno, J., Chi, X., Walter, D., Lavric, J. V., Moran-Zuloaga, D., Ditas, F., Pöhlker, C., Brito, J., Carbone, S., Artaxo, P. and Andreae, M. O.: Modeling investigation of light-absorbing aerosols in the Amazon Basin during the wet season, Atmos. Chem. Phys., 16(22),

Formatted: Font color: Black

Formatted: Normal, Border: Top: (No border), Bottom: (N border), Left: (No border), Right: (No border), Between : (border), Tab stops: 3.13", Centered + 6.27", Right

14775–14794, doi:10.5194/acp-16-14775-2016, 2016.

Wang, Y., Pang, Y., Huang, J., Bi, L., Che, H., Zhang, X. and Li, W.: Constructing Shapes and Mixing Structures of Black Carbon Particles With Applications to Optical Calculations, J. Geophys. Res. Atmos., 126(10), 1–15, doi:10.1029/2021JD034620, 2021.

Wennberg, P. O., Bates, K. H., Crounse, J. D., Dodson, L. G., McVay, R. C., Mertens, L. A., Nguyen, T. B., Praske, E., Schwantes, R. H., Smarte, M. D., St Clair, J. M., Teng, A. P., Zhang, X. and Seinfeld, J. H.: Gas-Phase Reactions of Isoprene and Its Major Oxidation Products, Chem. Rev., 118(7), 3337–3390, doi:10.1021/acs.chemrev.7b00439, 2018.

Whitehead, J. D., Darbyshire, E., Brito, J., Barbosa, H. M. J., Crawford, I., Stern, R., Gallagher, M. W., Kaye, P. H., Allan, J. D., Coe, H., Artaxo, P. and McFiggans, G.: Biogenic cloud nuclei in the central Amazon during the transition from wet to dry season, Atmos. Chem. Phys., 16(15), 9727–9743, doi:10.5194/acp-16-9727-2016, 2016.

Wiedensohler, A., Birmili, W., Nowak, A., Sonntag, A., Weinhold, K., Merkel, M., Wehner, B., Tuch, T., Pfeifer, S., Fiebig, M., Fjäraa, a. M., Asmi, E., Sellegri, K., Depuy, R., Venzac, H., Villani, P., Laj, P., Aalto, P., Ogren, J. a., Swietlicki, E., Williams, P., Roldin, P., Quincey, P., Hüglin, C., Fierz-Schmidhauser, R., Gysel, M., Weingartner, E., Riccobono, F., Santos, S., Grüning, C., Faloon, K., Beddows, D., Harrison, R., Monahan, C., Jennings, S. G., O'Dowd, C. D., Marinoni, A., Horn, H.-G., Keck, L., Jiang, J., Scheckman, J., McMurry, P. H., Deng, Z., Zhao, C. S., Moerman, M., Henzing, B., de Leeuw, G., Löschau, G. and Bastian, S.: Mobility particle size spectrometers: harmonization of technical standards and data structure to facilitate high quality long-term observations of atmospheric particle number size distributions, Atmos. Meas. Tech., 5(3), 657–685, doi:10.5194/amt-5-657-2012, 2012.

Wu, L., Li, X., Kim, H., Geng, H., Godoi, R. H. M., Barbosa, C. G. G., Godoi, A. F. L., Yamamoto, C. I., Souza, R. A. F. De, Pöhlker, C., Andreae, M. O. and Ro, C.: Single-particle characterization of aerosols collected at a remote site in the Amazonian rainforest and an urban site in Manaus, Brazil, Atmos. Chem. Phys., 1221–1240, doi:10.5194/acp-19-1221-2019, 2019.

Xu, L., Guo, H., Boyd, C. M., Klein, M., Bougiatioti, A., Cerully, K. M., Hite, J. R., Isaacman-VanWertz, G., Kreisberg, N. M., Knote, C., Olson, K., Koss, A., Goldstein, A. H., Hering, S. V., de Gouw, J., Baumann, K., Lee, S.-H., Nenes, A., Weber, R. J. and Ng, N. L.: Effects of anthropogenic emissions on aerosol formation from isoprene and monoterpenes in the southeastern United States, Proc. Natl. Acad. Sci., 112(1), 37–42, doi:10.1073/pnas.1417609112, ~~2015a~~2015.

~~Xu, L., Guo, H., Boyd, C. M., Klein, M., Bougiatioti, A., Cerully, K. M., Hite, J. R., Isaacman-VanWertz, G., Kreisberg, N. M., Knote, C., Olson, K., Koss, A., Goldstein, A. H., Hering, S. V, de Gouw, J., Baumann, K., Lee, S. H., Nenes, A., Weber, R. J. and Ng, N. L.: Effects of anthropogenic emissions on aerosol formation from isoprene and monoterpenes in the southeastern United States, Proc. Natl. Acad. Sci., 112(1), 37–42, doi:10.1073/pnas.1417609112, 2015b.~~

Yamasoe, H. A., Artaxo, P., Miguel, A. H. and Allen, A. G.: Chemical composition of aerosol particles from direct emissions of vegetation " res in the Amazon Basin : water-soluble species and trace elements, Atmos. Environ., 34, 2000.

Yáñez-Serrano, A. M., Nölscher, A., C., .. Williams, J., Wolff, S., Alves, E., Martins, G. a., Bourtsoukidis, E., Brito, J., Jardine, K., Artaxo, P. and Kesselmeier, J.: Diel and seasonal changes of biogenic volatile organic compounds within and above an Amazonian rainforest, Atmos. Chem. Phys., 15(6), 3359–3378, doi:10.5194/acp-15-3359-2015, 2015.

Yu, H., Wu, C., Wu, D. and Yu, J. Z.: Size distributions of elemental carbon and its contribution to light extinction in urban and rural locations in the pearl river delta region, China, Atmos. Chem. Phys., 10(11), 5107–5119, doi:10.5194/acp-10-5107-2010, 2010.

Zaveri, R. A., Wang, J., Fan, J., Zhang, Y., Shilling, J. E., Zelenyuk, A., Mei, F., Newsom, R., Pekour, M., Tomlinson, J., Comstock, J. M., Shrivastava, M., Fortner, E., Machado, L. A. T., Artaxo, P. and Martin, S. T.: Rapid growth of anthropogenic organic nanoparticles greatly alters cloud life cycle in the Amazon rainforest, Sci. Adv., 8(2), 1–17, doi:10.1126/sciadv.abj0329, 2022.

Zhang, Q., Jimenez, J. L., Canagaratna, M. R., Ulbrich, I. M., Ng, N. L., Worsnop, D. R. and Sun, Y.: Understanding atmospheric organic aerosols via factor analysis of aerosol mass spectrometry: A review, Anal. Bioanal. Chem., 401(10), 3045–3067, doi:10.1007/s00216-011-5355-y, 2011.

Zhang, Y., Zhi, G., Jin, W., Wang, L., Guo, S., Shi, R., Sun, J., Cheng, M., Bi, F., Gao, J., Zhang, B., Wu, J., Shi, Z., Liu, B., Wang, Z. and Li, S.: Differing effects of escalating pollution on absorption and scattering efficiencies of aerosols: Toward co-beneficial air quality enhancement and climate protection measures, Atmos. Environ., 232(April), 117570, doi:10.1016/j.atmosenv.2020.117570, 2020.

Formatted: Font color: Black

Formatted: Normal, Border: Top: (No border), Bottom: (N border), Left: (No border), Right: (No border), Between : (border), Tab stops: 3.13", Centered + 6.27", Right

Zhu, C. S., Cao, J. J., Ho, K. F., Antony Chen, L. W., Huang, R. J., Wang, Y. C., Li, H., Shen, Z. X., Chow, J. C., Watson, J. G., Su, X. li, Wang, Q. yuan and Xiao, S.: The optical properties of urban aerosol in northern China: A case study at Xi'an, Atmos. Res., 160, 59–67, doi:10.1016/j.atmosres.2015.03.008, 2015.

Formatted: Normal, Space After: 10 pt, Border: Top: (No border), Bottom: (No border), Left: (No border), Right: (No border), Between : (No border)

Formatted: Font color: Black

Formatted: Normal, Border: Top: (No border), Bottom: (No border), Left: (No border), Right: (No border), Between : (No border), Tab stops: 3.13", Centered + 6.27", Right

45